CAPITAL UNIVERSITY OF SCIENCE AND TECHNOLOGY, ISLAMABAD

Simulations of Natural Convective Flow in a Square Cavity with Nonlinear Thermal Radiation

by

Bilal Ahmad

A thesis submitted in partial fulfillment for the degree of Master of Philosophy

in the

Faculty of Computing
Department of Mathematics

2018

Dedicated to ones who gave me life and grew me up

Those angels who were always my supportive.

I owe them each moments of my life and praise

them in every breath.

Dedicated to the most holy person, Mother

GULZAR BIBI

And the dearest person, Father

ZIA ULLAH.

CAPITAL UNIVERSITY OF SCIENCE & TECHNOLOGY

ISLAMABAD

CERTIFICATE OF APPROVAL

Simulations of Natural Convective Flow in a Square Cavity with Nonlinear Thermal Radiation

by

Bilal Ahmad

MMT153017

THESIS EXAMINING COMMITTEE

S. No.	Examiner	Name	Organization
(a)	External Examiner	Dr. Manshoor Ahmed	C.U.I, Islamabad
(b)	Internal Examiner	Dr. Muhammad Sagheer	C.U.S.T, Islamabad
(c)	Supervisor	Dr. Shafqat Hussain	C.U.S.T, Islamabad

Dr. Shafqat Hussain

Thesis Supervisor

October, 2018

Dr. Muhammad Sagheer

Head

Dept. of Mathematics

October, 2018

Dr. Muhammad Abdul Qadir

Dean

Faculty of Computing

October, 2018

Author's Declaration

I, **Bilal Ahmad** hereby state that my M. Phil thesis titled "**Simulations of Natural Convective Flow in a Square Cavity with Nonlinear Thermal Radiation**" is my own work and has not been submitted previously by me for taking any degree from Capital University of Science and Technology, Islamabad or anywhere else in the country/abroad.

At any time if my statement is found to be incorrect even after my graduation, the University has the right to withdraw my M. Phil Degree.

(Bilal Ahmad)

Registration No: MMT153017

Plagiarism Undertaking

I solemnly declare that research work presented in this thesis titled *"Simulations of Natural Convective Flow in a Square Cavity with Nonlinear Thermal Radiation"* is solely my research work with no significant contribution from any other person. Small contribution/help wherever taken has been dully acknowledged and that complete thesis has been written by me.

I understand the zero tolerance policy of the HEC and Capital University of Science and Technology towards plagiarism. Therefore, I as an author of the above titled thesis declare that no portion of my thesis has been plagiarized and any material used as reference is properly referred/cited.

I undertake that if I am found guilty of any formal plagiarism in the above titled thesis even after award of M. Phil Degree, the University reserves the right to withdraw/revoke my M. Phil degree and that HEC and the University have the right to publish my name on the HEC/University website on which names of students are placed who submitted plagiarized work.

(Bilal Ahmad)

Registration No: MMT153017

Acknowledgements

All the praise and appreciation are for almighty **ALLAH** who is the most benefi-
cent and the most merciful. He created the universe and blessed the mankind with
intelligence and wisdom to explore His secrets. Countless respect and endurance
for **Prophet Muhammad** (Peace Be Upon Him), the fortune of knowledge, who
took the humanity out of ignorance and showed the right path.

I would like to show my gratitude and immeasurable respect to my supervisor
Dr. Shafqat Hussain, Associate Professor, Capital University of Science and
Technology, Islamabad who suggested the problem, extended all facilities and pro-
vided inspiring guidance for the successful completion of my research work. I deem
it as my privilege to work under his able guidance.

Special thanks to my teacher **Dr. Muhammad Sagheer**, Professor, Capital
University of Science and Technology, Islamabad for his kind, friendly, encourag-
ing and enthusiastic attitude which gave me courage of facing ups and downs of
the process. I have enjoyed every moment of insightful discussion with him.

Without any exaggeration again, I am extremely indebted to **Dr. Khalid Mehm-
ood**, all research scholars, friends and colleagues in Mathematics lab for their ever
friendly behavior, inspiring guidance and encouraging environment during the re-
search period.

At this juncture, I pay my deep regards to my beloved parents, teachers **Qari
Saleem**, **Ch Basharat**, **M. Nasir**, **Farooq Malik** and specially my sisters for
their selfless care, love and prayers that made me able to achieve this goal. May
Allah bless them all.

Bilal Ahmad

Abstract

The aim of this thesis is to analyze the influence of non-linear thermal radiation parameter on two dimensional, steady and incompressible natural convective flow in a square tilted cavity. The cavity is assumed with adiabatic conditions on the top and bottom walls, heated on the left wall and cooled on the right wall. The governing equations for the heat exchange and fluid flow have been solved numerically by utilizing Galerkin weighted residual finite element method. In particular, velocity and temperature fields are discretized using the biquadratic Q_2 element and for pressure discontinuous P_1 element is utilized. The impact of physical parameters on the heat and fluid flow are discussed and analyzed in terms of streamlines, isotherms and some useful plots. Effect of the physical parameters in specified ranges such as thermal radiation parameter ($Rd = 0 - 3$), Prandtle number ($Pr = 0.025, 6.2, 0.71$ and 998), Rayleigh number ($Ra = 10^3 - 10^5$) and inclination angle ($\Phi = 15°, 30°, 60°, 75°$) on the fluid flow and heat transfer has been investigated.

Contents

List of Figures

List of Tables

Abbreviations

BVP **B**oundary **V**alue **P**roblem

FEM **F**inite **E**lement **M**ethod

PDEs **P**artial **D**ifferential **E**quations

Symbols

a_R Rosseland mean absorption coefficient (m^{-1})

c_p specific heat constant $(J\ kg^{-1}\ K^{-1})$

g gravitational acceleration $(m\ s^{-2})$

k thermal conductivity $(kg\ m\ s^3\ K-1)$

L length of the square cavity (m)

N_r temperature ratio $(\frac{T_h}{T_c})$

Nu local Nusselt number

Nu_{avg} averaged Nusselt number

p pressure (Pa)

P non-dimensional pressure

Pr Prandtl number $(\frac{\nu}{\alpha})$

Q heat energy (J)

q_r radiative heat flux (W/m^2)

Ra Rayleigh number $(\frac{g\beta(T_h - T_c)L^3 Pr}{\nu^2})$

Rd thermal radiation parameter $(\frac{4\sigma_* T_c^3}{a_R \kappa})$

Re Reynolds number $(\frac{LU}{\nu})$

s displacement (m)

T fluid temperature (K)

T_h hot left wall temperature (K)

T_c cold right wall temperature (K)

u velocity in x-direction $(m\ s^{-1})$

U dimensionless velocity component in x-direction

v velocity in y-direction $(m\ s^{-1})$

V	dimensionless velocity component in y-direction
(x, y)	dimensional co-ordinates
(X, Y)	dimensionless (x, y) coordinates
n	unit normal vector

Greek symbols

α	thermal diffusivity $(m^2\ s^{-1})$
β	thermal expansion coefficient (K^{-1})
Φ	inclination angle with positive direction of X axis
θ	non-dimensional temperature $(T - T_c/T_h - T_c)$
ρ	fluid density (kg/m^3)
μ	dynamic viscosity $(kg\ m^{-1}\ s^{-1})$
ν	kinematic viscosity $(m^2\ s^{-1})$
ΔT	temperature gradient (K)
σ_*	Stefan-Boltzman constant $(W/m^2 K^4)$

Subscripts

avg	average
c	cold
h	hot

Chapter 1

Introduction

The transfer of heat by the movement of fluids from one place to another is called convective heat transfer. Convective heat transfer is combination of heat diffusion and bulk fluid flow simultaneously. The study of natural convection has been extensively investigated and has gained considerable attention in various fields of engineering including thermoelastic damping [1], cooling of devices [2], welding [3] and many more. Convective heat transfer has wide applications on industrial level e.g., heat exchanger [4], solar collectors [5], room ventilation [6], chemical reactor [7] and many others because of its simplicity and low cost. Due to this tremendous and widespread expansion of free convection applications, many researchers are incessantly investigating the convective heat flow in various physical systems such as magnetohydrodynamics convection [8], forced convection [9], convection of nanofluids [10], etc. Natural convection in cavities with heat generated fluids has been extensively studied [11–13]. Convective flow within square cavity is one of the most investigated solution of Naiver-Stokes equations which plays an significant role in the study of fluid dynamics. The name of Navier-Stokes is derived from Claud Luis Navier and George Gabriel Stokes. Navier-Stokes equations have lots of practical applications in physical world.

Basak *et al.* [14] performed the simulations on natural convective flow in tilted square enclosure. The impact of inclination angles on a fluid flow via streamlines,

heat flow via heatlines and entropy genaration because of transfer of heat and fluid friction throughout free convection inside a tilted square enclosure was analyzed. The enclosure is surrounded by two adiabatic walls, cold (CB) and hot (DA) wall. Numerical results are presented for various parameters. The Galarkin finite element methods was utilized in order to explain the numerical procedure of nonlinear partial differential equation. The convective heat transfer was observed both analytically and numerically in a square enclosure.

Ozoe *et al.* [15] investigated the heat transfer rate experimentally as well as numerically within an inclined cavity in which the inclined side is kept at constant hot temperature while the opposite side was provided with low temperature. Rasoul et al. [16] numerically inspected the influence of inclined cavity on laminar natural convection for various Prandtl and Rayleigh numbers. It was concluded that an increase in the inclination angle results into a decrease in the Nu_{avg} number, irrespective of Prandtl and Rayleigh numbers. More comprehensive study on free convection with the effect of inclination angle was also examined by Cotton *et al.* [17], Farhny and Kuran [18] and Hamady *et al.* [19] for various parameters and arbitrary inclination angles. Shiralker and Tien [20] investigated the simultaneously differential heating effect of the vertical wall as well as the horizontal wall of the square enclosure. Numerical study of the free convective flow in a rectangular enclosure cooled from one side and heated on bottom was studied by Ganzoralli and Milanez [21]. Khanafer *et al.* [22] numerically inspected free convection in square enclosure filled with alumina-water nanofluid. It was concluded that depending on the model used, the heat transfer may increase or decrease for viscosity and thermal conductivity of the nanofluids. Selimefendigil and Öztop [23] also inspected the problem of free convection numerically by using cooling and heating sinusoidal temperature profiles on one side in a tilted enclosure filled with water-based nanofluid.

Similarly, Abu-Nada [24] studied the enhancement in transfer of heat in a differentially heated enclosure of natural convection using varying properties of alumina-water and copper-water nanofluid. For high Rayleigh numbers, their results showed that the Nu_{avg} was more effective to the models of viscosity rather than to the models of thermal conductivity. Cianfrini *et al.* [25] investigated the influence of the angle of inclination on heat transport in a square enclosure with opposite walls being differentially heated. They obtained the significant effect of the angle of inclination on overall heat transport in both x-direction and y-direction which is comparatively larger than that of untilted case.

Thermal radiation is electromagnetic radiation produced by the thermal motion of charged particles in matter. Mehmood *et al.* [26] numerically investigated the MHD mixed convection in alumina-water nanofluid-filled square porous cavity using KKL model considering the effect of non-linear thermal radiation and inclined magnetic field. Galarkin finite elements method was adopted to explain the governing equation. It was observed that radiation parameter declines the heat transfer due to hot wall. Shekar and Kishan [27] examined the natural convective heat transfer in a porous square enclosure filled with nano-fluids in the presence of thermal radiation. They noticed that radiation parameter favours the thermal boundary layer thickness.

Thermal radiation is usually produced as an outcome of emission by hot wall. It is important to mention here that some practical applications of thermal radiation in sciences and engineerings exist. Mahapatra *et al.* [28] analyzed free convection in a square enclosure with the impact of linear thermel radiation. Ghalambaz *et al.* [29] inspected the free convection in a porous square cavity filled by a nanofluid considering linear thermal radiations and viscous dissipations effect. It was noticed that heat transfer increases with thermal radiation parameters. Sheikholeslami *et al.* [30] performed numerical simulation for MHD natural convection of alumina-water nanofluid filled enclosure under the influence of linear thermal radiations.

1.1   Thesis Contributions

The aim of this thesis is to examine the natural convection heat flow with non-
linear thermal radiation inside an inclined square cavity. The system of governing
equations is solved by using Galerkin finite element technique, particularly Q_2 of
3rd order accuracy is used to discretize the velocity as well as temperature and
discontinuous P_1 element of 2nd order accuracy is used for the pressure [31]. The
numerical simulations of the dimensionless velocity and temperature are analyzed
by using the streamlines and isotherms, respectively, while the $Nuavg$ number is
viewed by some useful plots against different physical parameters and inclination
angle.

1.2 Thesis Outline

This thesis is further organized into four chapters.

Chapter 2 contains some basic definitions, concepts and physical laws related to fluid dynamics that are helpful in understanding the work in the subsequent chapters.

Chapter 3 presents the review of the research paper [14]. In this chapter, the steady natural convective flow is inspected in square cavity inclined at different angles. A suitable transformation is used to convert equations governing the flow in to non-dimensional form and solve these nonlinear coupled PDEs numerically using Galerkin finite element method. Numerical results are calculated and analyzed for various parameters such as Pr, Ra and inclination angle Φ.

Chapter 4 extends the work of Basak *et al.* [14] with the idea of non-linear thermal radiations. The non-dimensional governing equations are discretized using biquadratic element Q_2, for velocity and temperature, and discontinuous P_1 element for pressure. Simulations are performed for various parameters such as non-linear thermal radiation, Pr, Φ, Rd and Ra, and their corresponding influence can be seen through streamlines and isotherms.

Chapter 5 summarizes the conclusion of the present work.

Bibliography contains all the references used in thesis are listed at the end.

Chapter 2

Basic Definitions and Governing Equations

In this chapter, some basic concepts, terminologies, definitions and governing laws [32] are explained, which will be helpful in continuing this work for the next chapters. The procedure of finite element method is also explained and illustrated by a two dimensional Poisson problem.

2.1 Fluid Related Terminologies

Definition 2.1. (Fluid)

The material which alters continuously by the effect of shear stress is called fluid. It doesn't matter that what kind of shear stress it is.The shape of the fluid is also changed through the act of shear stress. Liquids and gases are the examples of fluids.

Definition 2.2. (Fluid Mechanics)

The area of physical sciences in which we study the action of a fluid in static or dynamic condition is called fluid mechanics. It is further categorised into fluid statics and fluid dynamics.

Definition 2.3. (Fluid Statics)

From the family of fluid mechanics, a branch that deals with the fluid and its characteristics at a fixed position, is called fluid statics.

Definition 2.4. (Fluid Dynamics)

The branch that covers the properties of fluid in the state of motion from one place to another is called fluid dynamics.

Definition 2.5. (Density)

Concentration of mass per unit volume is termed as density of material. Symbolically, it is represented by greek letter ρ and mathematically written as

$$\rho = \frac{m}{V}. \tag{2.1}$$

Here V and m are the volume and mass of the material, respectively.

Definition 2.6. (Pressure)

The component of applied force perpendicular to the surface of an object per unit area is termed as pressure. It is represented by P and mathematically, it is written as

$$P = \frac{F}{A}, \tag{2.2}$$

where F and A denote the applied force and area of the surface, respectively.

Definition 2.7. (DynamicViscosity)

The extent which measures the resistance of fluid tending to cause the fluid to flow is called dynamic viscosity, also known as absolute viscosity. This resistance arises from the attractive forces between the molecules of the fluid. Usually liquids and gasses have non-zero viscosity. It is denoted by symbol μ_D and mathematically, it can be written as

$$\mu_D = \frac{\text{shear stress}}{\text{shear strain}}. \tag{2.3}$$

Here μ_D is called the coefficient of viscosity. Unit of viscosity in SI system is kg/ms or Pascal-second.

Definition 2.8. (Kinematic Viscosity)

It is the ratio of the dynamic viscosity to the density. Symbolically, it can be written as ν. Mathematically,

$$\nu = \frac{\mu_D}{\rho}, \tag{2.4}$$

where, the dimension of kinematic viscosity is $[L^2 T^{-1}]$ and its unit in SI system is m^2/s.

Definition 2.9. (Stress)

Stress is a force which acts parallel or perpendicular to the material surface per unit its area and is denoted by σ. It is a tensor quantity. Mathematically, it can be written as;

$$\sigma = \frac{F}{A}, \tag{2.5}$$

where F represents force and A denotes area.

Definition 2.10. (Shear Stress)

It is a type of stress in which force vector acts parallel to the material surface or cross section of a material.

Definition 2.11. (Normal stress)

Normal stress is a type of stress in which force vector acts perpendicular to the surface of the material or cross section of a material.

Definition 2.12. (Yield Stress)

The property of material at which a matter begins to deform physically until the force acting on it and will back to its original form when the applied force is released.

2.2 Classification of Fluids

Definition 2.13. (Ideal Fluid)

An ideal fluid is defined as the fluid which is incompressible and has no viscosity (μ=0). In other words, the fluid which does not lose kinetic energy is called ideal fluid. It requires no viscosity due to non-availability of shear force. It is also known as inviscid fluid.

Definition 2.14. (Real Fluid)

The fluid which is compressible in nature and contains some viscosity ($\mu > 0$) is said to be real or viscous fluid. As the fluid moves, certain amount of resistance is always offered by the fluid. It is known as viscous fluid or viscid fluid.

Definition 2.15. (Newtonian Fluid)

The fluid for which the shear stress varies directly and linearly as the deformation rate is known as Netownian fluid. Shear stress of Newtonian fluid is mathematically defined as

$$\tau_{yx} \propto \left(\frac{du}{dy} \right) \ ,$$

$$\tau_{yx} = \mu_D \left(\frac{du}{dy} \right) \ , \tag{2.6}$$

where τ_{yx} is shear stress and u denotes the x-component of velocity and μ_D denotes the dynamic viscosity. The common examples of Newtonian fluids are mercury, air, water, glycerol, oxygen, gas, alchohol and milk etc.

Definition 2.16. (Non − Newtonian Fluid)

The fluids for which the shear stress does not vary linearly as the deformation rate are known as Non-Newtonian Fluids. Mathematically, it can be expressed as

$$\tau_{yx} \propto \left(\frac{du}{dy} \right)^m \ , \ \ m \neq 1$$

$$\tau_{yx} = \mu \left(\frac{du}{dy} \right)^m \ , \tag{2.7}$$

where μ denotes the apparent viscosity and m is the index of the flow performance. The common examples are toothpaste, ketchup, starch suspension, custard, shampoo, paint and blood etc. Note that for $m = 1$, the equation (2.6) reduces to the Newton's law of viscosity.

2.3   Types of Flows

Definition 2.17. (Flow)

An object exhibits the flow if unbalanced forces lead to an unbounded distortion. Several types of flow are as follow:

Definition 2.18. (Laminar Flow)

In fluid dynamics, laminar flow occurs when a flow is in parallel/closed channel or flat plates with no interruption between the plates. Typically, each particle has a definite path and the particles of the path in the fluid don't cross each other. Rising of cigarette smoke is an example of laminar flow.

Definition 2.19. (Turbulent Flow)

When the fluid undergoes irregular fluctuations or flowing faster, this type of flow (liquid or gas) is called turbulent flow. Turbulent flow moves randomly in any direction and has no definite path and cannot be handled easily. It goes changes both in magnitude and direction.

Definition 2.20. (Steady Flow)

The flow that doesn't change with respect to time is called steady flow. Mathematically, it can be written as

$$\frac{d\eta^*}{dt} = 0, \tag{2.8}$$

where η^* is any fluid property.

Definition 2.21. (Unsteady Flow)

The flow that continuously changes with respect to time, is expressed as unsteady flow. Mathematically, it can be written as

$$\frac{d\eta^*}{dt} \neq 0, \tag{2.9}$$

where η^* is fluid property.

Definition 2.22. (Compressible Flow)

The flow in which the material density varies during fluid flow is said to be compressible flow. Compressible fluid flow is used in high-speed jet engines, aircraft, rocket motors also in high-speed usage in a planetary atmosphere, gas pipelines and in commercial fields. Mathematically, it is expressed as

$$\rho(x, y, z, t) \neq c, \tag{2.10}$$

where c is constant.

Definition 2.23. (Incompressible Flow)

A type of fluid flow in which material density during the flow remains constant is said to be incompressible flow. Mathematically, defined as

$$\rho(x, y, z, t) = c, \tag{2.11}$$

where c is constant.

Definition 2.24. (Uniform Flow)

The flow in which the velocity of each fluid particle remains unchanged from point to point at any given instant of time, having same direction as well as magnitude during fluid motion called as uniform flow. It is mathematically expressed as

$$\frac{\partial \mathbf{V}}{\partial s} = 0, \tag{2.12}$$

where $\mathbf{V}$ is the velocity and s is the displacement in any direction.

Definition 2.25. (Nonuniform Flow)

The flow in which the velocity of fluid particle changes from point to point at any given instant of time, either having different direction or different magnitude during fluid motion called as uniform flow. Mathematically, it is expressed as

$$\frac{\partial \mathbf{V}}{\partial s} \neq 0, \tag{2.13}$$

where $\mathbf{V}$ is the velocity and s is the displacement.

Definition 2.26. (Internal Flow)

Fluid flow which is confined by the solid surface. The examples of the internal flow are the flow through pipes or glass.

Definition 2.27. (External Flow)

A type of flow which is not bounded by the solid surface.Water flow in the rivers and oceans are the examples of external flow.

2.4 Heat Transfer and Related Properties

Definition 2.28. (Heat Transfer)

It is the energy transfer from high temperature reservior to low temperature reservior due to difference of temperature. When there is a difference of temperature in a medium or between media, heat transfer must take place. This phenomenon can occur in term of following three mechanisms.

Definition 2.29. (Conduction)

In this process, the transmission of heat through matter occurs by the interaction of free electrons and molecules. In other words, when free electrons move from one object to another due to molecular interaction without disturbance or motion of material as a whole is known as a conduction. Mathematically, it is expressed as

$$q = -\kappa A \left(\frac{\triangle T}{\triangle n} \right), \tag{2.14}$$

where κ denotes the constant of thermal conductivity, A denotes area and $\frac{\triangle T}{\triangle n}$ denotes gradient of temperature respectively.

Definition 2.30. (Convection)

The mechanism in which fluid is forced by external processes and when thermal energy expands in gravitational fields by the interaction of buoyancy forces is called convection. In other words, convection is the process in which heat transfer occurs by the movement of fluids from one place to another such as air, water etc. The

convection phenomena take place through diffusion or advection. Mathematically, it is expressed as

$$q = hA(T_s - T_\infty), \tag{2.15}$$

where h, A, T_s and T_∞ represent the heat transfer coefficient, the area, the temperature of the surface and the temperature away from the surface respectively. It is further categorised into natural convection, force convection and mixed convection.

Definition 2.31. (Force Convection)

Force convection is such type of communication for which motion of fluid is produced by an external source (like pump, fan etc) is categorized as force convection. It is also used in machines, air conditioning, central heating and in many other turbines.

Definition 2.32. (Natural Convection)

When motion of fluid is not generated by an independent source then it is said to be natural convection or called free convection. Simplifying more, it occurs due to the temperature gradient difference having effect on density. Natural convection can only exists in gravitational field.

Definition 2.33. (Mixed Convection)

A flow mechanism which is simultaneously contributed by both force and free convection processes and acting simultaneously. Mixed convection is always realized when small number of velocities are characterized on colling and heating of walls.

Definition 2.34. (Radiation)

In radiation process, heat is transferred through electromagnetic waves or rays. In fluids both convection and radiation are most significant in flow of heat but in solids radiation is usually negligible. For example, if a material object is placed under sun rays, after a while the material object is heated. Such phenomena takes place due to radiation. Mathematically, it can be written as

$$q = E\sigma A[(\triangle T)^4], \tag{2.16}$$

where E, σ, $(\triangle T)^4$, A, q are the emissivity of the material, the constant of Stefan Boltzmann (5.670×10^{-8}), the variation of the temperature, the area and the heat transfer respectively.

Definition 2.35. (**Thermal Conductivity**)

The property of a substance which measures the ability to transfer heat is called thermal conductivity, denoted by k. Mathematically, it can be written as

$$\frac{dQ}{dt} = -kA\frac{dT}{dx}, \tag{2.17}$$

where $\frac{dQ}{dt}$, A, $\frac{dT}{dx}$ are the heat flow, the area and the temperature gradient, respectively. Thermal conductivity of most liquids decreases with the increase of temperature except water. Its SI unit is $\frac{Kg.m}{s^3.K}$ and the dimension is $[MLT^{-3}\theta^{-1}]$.

Definition 2.36. (**Thermal Diffusivity**)

The ratio of the unsteady heat conduction (k) of a substance to the product of specific heat capacity (c_p) and density (ρ) is called thermal diffusivity. It quantify the ability of a substance to transfer heat rather to store it. Mathematically, it can be written as

$$\alpha = \frac{k}{\rho c_p}. \tag{2.18}$$

2.5 Basic Governing Equations

2.5.1 Continuity Equation

The equation of continuity is derived from the mass conservation law and mathematically, it is expressed by

$$\frac{\partial \rho}{\partial t} + \nabla.(\rho \mathbf{V}) = 0, \tag{2.19}$$

where t is the time. If fluid is an incompressible, then it is expressed by

$$\nabla.\mathbf{V} = 0. \tag{2.20}$$

2.5.2 Momentum Equation

Each particle of fluid obeys Newton's second law of motion which is at rest or in steady state or accelerated motion. This law states that the combination of all applied external forces working on an object is equal to the time rate of change of its linear momentum. In vector notation this law is expressed as

$$\rho \frac{D\mathbf{V}}{Dt} = \text{div } \tau + \rho b, \tag{2.21}$$

For Navier-Stokes equation

$$\tau = -pI + \mu A_1, \tag{2.22}$$

where A_1 is the tensor and first time it was produced by Rivlin-Erickson.

$$A_1 = \text{grad } \mathbf{V} + (\text{grad } \mathbf{V})^t, \tag{2.23}$$

In the above equations, $\frac{D}{Dt}$ denote the material time derivative or total derivative, $\mathbf{V}$ denote velocity field, ρ denote density, τ here denotes the Cauchy stress tensor, b the body forces, p is the pressure and μ the dynamic viscosity.

The stress tensor τ is expressed in the matrix form as

$$\tau = \begin{pmatrix} \sigma_{xx} & \tau_{yx} & \tau_{zx} \\ \tau_{xy} & \sigma_{yy} & \tau_{zy} \\ \tau_{xz} & \tau_{yz} & \sigma_{zz} \end{pmatrix}, \tag{2.24}$$

where σ_{xx}, σ_{yy} and σ_{zz} are normal stresses, others wise the shear stresses. For two-dimensional flow, we have $\mathbf{V} = [u(x,y,0), v(x,y,0), 0]$ and thus

$$\text{grad } \mathbf{V} = \begin{pmatrix} \frac{\partial u}{\partial x} & \frac{\partial u}{\partial y} & 0 \\ \frac{\partial v}{\partial x} & \frac{\partial v}{\partial y} & 0 \\ 0 & 0 & 0 \end{pmatrix}, \tag{2.25}$$

$$\frac{\partial u}{\partial t} + u\frac{\partial u}{\partial x} + v\frac{\partial u}{\partial y} = -\frac{1}{\rho}\frac{\partial p}{\partial x} + \nu\left(\frac{\partial^2 u}{\partial x^2} + \frac{\partial^2 u}{\partial y^2}\right), \tag{2.26}$$

Similarly, we repeat the above process for Y component as follows:

$$\frac{\partial v}{\partial t} + u\frac{\partial v}{\partial x} + v\frac{\partial v}{\partial y} = -\frac{1}{\rho}\frac{\partial p}{\partial y} + \nu\left(\frac{\partial^2 v}{\partial x^2} + \frac{\partial^2 v}{\partial y^2}\right), \tag{2.27}$$

2.5.3 Energy Equation

The energy equation is

$$\rho c_p \left(\frac{\partial}{\partial t} + \mathbf{V}\nabla\right) T = k\nabla^2 T + \tau L, \tag{2.28}$$

where (c_p) denotes the specific heat constant, ρ the density of basic fluid, L denotes the rate of strain tensor and T the temperature of the fluid. The Cauchy stress tensor τ for viscous and incompressible fluid is expressed by

$$\tau = -pI + \mu A_1, \tag{2.29}$$

where A_1 is the tensor, p the pressure and μ the dynamic viscosity.

2.6 Dimensionless Numbers

Definition 2.37. (Reynolds Number (Re))

It is the most significant dimensionless number which is used to identify the different flow behaviors like laminar or turbulent flow. It helps to measure the ratio between inertial force and the viscous force. Mathematically,

$$Re = \frac{LU}{\nu}, \tag{2.30}$$

where L represents the characteristics length, U denotes the free stream velocity and ν stands for kinematic viscosity.

Definition 2.38. (Prandtl Number (Pr))

It is the relationship between the momentum diffusivity (ν) and thermal diffusivity (α). Mathematically it can be expressed as,

$$Pr = \frac{\nu}{\alpha} \implies \frac{\mu/\rho}{\kappa/(c_p\rho)} \implies \frac{\mu c_p}{\kappa}, \tag{2.31}$$

where μ is the dynamic viscosity, c_p stands for the specific heat constant and κ denotes thermal conductivity. The relative thickness of thermal and momentum boundary layer are controlled by Prandtl number.

Definition 2.39. (Nusselt Number (Nu))

The dimensionless number, used in heat transfer, is the ratio of convective to conductive heat transfer to the boundary. Mathematically,

$$Nu = \frac{hL}{\kappa}. \tag{2.32}$$

Here h represents the convective heat transfer, L denotes characteristics length and κ stands for thermal conductivity.

Definition 2.40. (Rayleigh Number (Ra))

It is the relationship between the kinematic diffusivity to heat diffusivity multiplied by the ratio of viscosity forces and buoyancy forces. It is a dimensionless number introduced by Lord Rayleigh. It is denoted by Ra and mathematically it can be written as

$$Ra = \frac{g\beta(T_h - T_c)L^3 Pr}{\nu^2}, \tag{2.33}$$

where g, β, L^3 and ν represents the gravitational accaleration, volume expansion coefficient, characteristic length and kinematic viscosity.

2.7   Finite Element Method (FEM)

It is a numerical scheme for finding the approximate solution of **PDEs**. It subdivides a huge problem into smaller parts, named as the finite elements. A finite

element method is simulated by a weak formulation, one or more solution algorithms and post processing procedure.

Definition 2.41. (Galerkin Finite Element Method)

The area of numerical analysis in which Galerkin method is the class of methods for converting the continuous problems into discrete problems. In principal, it is similar to variational method for applying parameters to the functional space, by interchanging the equations to the weak formulation [33]. It contains the following steps

1. Multiply both sides of governing equations of the problem by test function $w \, \epsilon \, W$, that is vanishing on the boundaries of the domain, where W is a test space.

2. Perform integration by parts such that some derivatives will be transferred from trial to test function.

3. Impose natural boundary conditions in the boundary integrals and essential boundary conditions to the trial and test spaces. This is called the variational formulation or weak formulation.

4. Generate triangulation or mesh. Divide the entire domain into non-overlapping elements. In one dimension, mesh is a set of points that is, $x_0 = 0, x_1, x_2, ...x_N = 1$, where x_i is called a node and $e_i = \{x_i, x_{i+1}\}$ is an element such that $e_i \bigcap e_j = \varphi$ for $i \neq j$. $h_i = x_i - x_{i-1}$ for $i = 0, 1, ...N$ is called mesh size.

5. Approximate the infinite dimensional trial space U and test space W by finite dimensional spaces U_h and W_h, respectively where U_h (finite dimensional space) $\subset U$ (solution space).

6. Choose the basis functions $\varphi_1, \varphi_2, ...\varphi_N$ of w_h, so that every test function $w_h \epsilon$ W_h can be written as $w_h = \sum w_i \varphi_i \epsilon \, W_h$ for $i = 1, ...N$.

7. Find $u_h \epsilon U_h$ such that $a(u_h, w_h) = b(w_h) \, \forall \, w_h = \sum w_i \varphi_i \, \epsilon W_h$ for $i = 1, ...N$,
   $\Rightarrow a(u_h, \varphi_i) = b(\varphi_i)$, where $i = 1, ..., N$.
   Substituting $u_h = \sum u_j \varphi_j$, for $j = 1, ...N$,

$a(\sum u_j \varphi_j, \varphi_i) = b(\varphi_i)$ for $i, j = 1, 2, 3..., N$,

$\Rightarrow \sum a(\varphi_j, \varphi_i) u_j = b(\varphi_i)$ for $i, j = 1, 2, 3..., N$.

where u_j are the solution values at the nodes. Also $a(u, w)$ is bilinear form and $b(w)$ is the linear form.

8. $(AU = B)$ is transformed which assembles the algebraic equation by varying i and j in row and column wise

To illustrate the method of Galerkin weighted residual, we consider the following example.

Example: Consider a 2D poisson problem

$$-\Delta u = f, \qquad in \ \Omega \tag{2.34}$$

$$u = 0, \qquad on \ \partial\Omega \tag{2.35}$$

where f is some known function and u is to find, Ω is domain of the problem which is open, bounded and connected and $\partial\Omega$ is the boundary.

The Variational Form:

- The exact solution u of the Eq. (2.34) should be twice continuously differentiable and satisfying Eq. (2.34). Let w be a test function such that $w(x) = 0$ on the boundary of the domain.

- Weighted residual integral statement of the poisson problem Eq. (2.34) is

$$-\int_\Omega w\Delta u \ d\Omega = \int_\Omega wf \ d\Omega, \tag{2.36}$$

- 2nd order derivatives of u can be reduced to 1st order by using Green's formula.

$$\int_{\partial\Omega} w\frac{\partial u}{\partial n} \ ds = \int_\Omega \nabla w \nabla u \ d\Omega + \int_\Omega w\Delta u \ d\Omega, \tag{2.37}$$

- Using Eq. (2.37) in Eq. (2.36) , we obtain

$$-\int_{\partial\Omega} w\frac{\partial u}{\partial n}\, ds + \int_{\Omega} \nabla w \nabla u\, d\Omega = \int_{\Omega} wf\, d\Omega, \qquad (2.38)$$

where the boundary integral vanishes due to the homogeneous boundary conditions, so we are left with

$$\int_{\Omega} \nabla w \nabla u\, d\Omega = \int_{\Omega} wf\, d\Omega, \qquad (2.39)$$

- Elemental weak form is

$$\int_{\Omega^e} \nabla w \nabla u\, d\Omega = \int_{\Omega^e} wf\, d\Omega, \qquad (2.40)$$

- In xy plane, Eq. (2.40) can be written as

$$\int_{\Omega^e} \left(\frac{\partial w}{\partial X}\frac{\partial u}{\partial X} + \frac{\partial w}{\partial Y}\frac{\partial u}{\partial Y}\right) d\Omega = \int_{\Omega^e} wf\, d\Omega, \qquad (2.41)$$

- Approximate solution over an element is

$$u^e = \sum_{j=1}^{NEN} u_j^e\, S_j^e(x,y). \qquad (2.42)$$

where S_j is a shape function and u_j are the solution values at nodes.

- Assemble local matrices into global matrix $(AU = B)$ and solve the system for U.

2.7.1 Advantages

Some of the basic features of Finite Element Method given below:

- Modeling of complex geometries and irregular shapes are easier [32].

- FEM can handle a wide variety of engineering problems [34].

Chapter 3

Simulations of Natural Convective Flow in a Square Cavity

In this chapter, we analyze the numerical study of the steady, incompressible and two dimensional natural convective flow in a square tilted cavity. By using an appropriate transformation, we reduce the system of governing equations such as continuity, momentum and energy equation into dimensionless coupled partial differential equations . These dimensionless governing equations have been solved by employing the finite element technique based on the Galerkin weighted residual method. The impact of governing parameters is analyzed through streamlines, isotherms and graphs. In this chapter, the review of the article [14] is presented.

3.1 Problem Description and Mathematical Formulation

Let us consider a two-dimensional, steady and incompressible free convective flow in a tilted square cavity. The schematic diagram of the problem under investigation with boundary conditions is shown in Figure 3.1. The cavity is tilted at

an inclination angle Φ with horizontal coordinate. The wall AD of the cavity is maintained hot at temperature T_h and the wall BC is maintained cold at temperature T_c, whereas two parallel walls DC and AB of the cavity are considered to be adiabatic. By means of Boussinesq approximation [35] change in density which arise due to variation in the fluid temperature is approximated while other physical properties of the density differences are ignored except in the buoyancy term. The equation of continuity, momentum and energy under the given assumptions read the following.

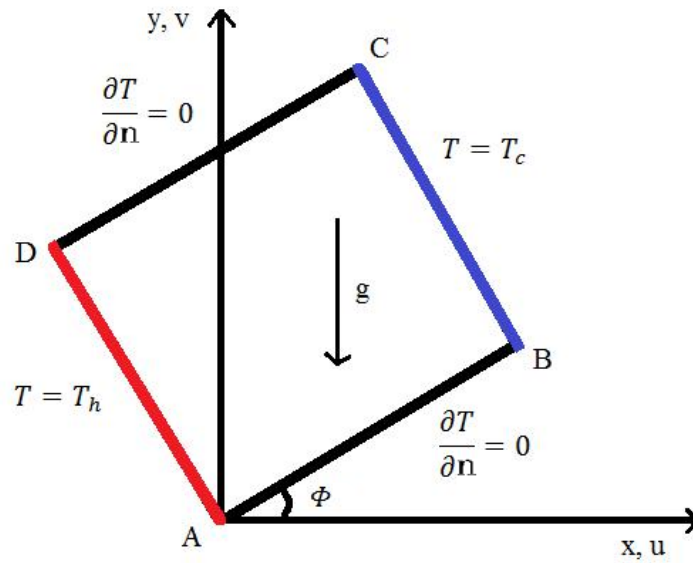FIGURE 3.1: Geometry of the problem.

Continuity equation:

$$\frac{\partial u}{\partial x} + \frac{\partial v}{\partial y} = 0, \tag{3.1}$$

x-momentum equation:

$$u\frac{\partial u}{\partial x} + v\frac{\partial u}{\partial y} = -\frac{1}{\rho}\frac{\partial p}{\partial x} + \nu\left(\frac{\partial^2 u}{\partial x^2} + \frac{\partial^2 u}{\partial y^2}\right) + g\beta(T - T_c)\sin\Phi, \tag{3.2}$$

y-momentum equation:

$$u\frac{\partial v}{\partial x} + v\frac{\partial v}{\partial y} = -\frac{1}{\rho}\frac{\partial p}{\partial y} + \nu\left(\frac{\partial^2 v}{\partial x^2} + \frac{\partial^2 v}{\partial y^2}\right) + g\beta(T - T_c)\cos\Phi, \qquad (3.3)$$

Energy equation:

$$u\frac{\partial T}{\partial x} + v\frac{\partial T}{\partial y} = \alpha\left(\frac{\partial^2 T}{\partial x^2} + \frac{\partial^2 T}{\partial y^2}\right). \qquad (3.4)$$

Here u, v denote the components of velocity along x and y direction respectively, p represents the pressure of the fluid, ρ is the fluid density, ν is kinematic fluid viscosity, acceleration due to gravity is g, the expansion coefficient is β, fluid temperature is T, T_c is the cold right wall temperature, Φ is an inclination angle and α is the thermal diffusivity.

For the velocity and temperature fields the dimensional form of boundary conditions on each wall of the cavity are given by

- On the horizontal walls AB and CD:

$$u(x, y) = 0, \quad v(x, y) = 0, \quad \frac{\partial T}{\partial \mathbf{n}} = 0 \qquad (3.5)$$

- On the right wall BC:

$$u(x, y) = 0, \quad v(x, y) = 0, \quad T = T_c \qquad (3.6)$$

- On the left Wall DA:

$$u(x, y) = 0, \quad v(x, y) = 0, \quad T = T_h \qquad (3.7)$$

where $\mathbf{n}$ denotes the normal vector.

3.1.1 Dimensionless Form of the Governing Equations

The dimensionless form of the Eqs. (3.1)-(3.4) has been obtained by using the following dimensionless parameters [14]

$$X = \frac{x}{L}, \quad Y = \frac{y}{L}, \quad U = \frac{uL}{\alpha}, \quad V = \frac{vL}{\alpha}, \quad P = \frac{pL^2}{\rho\alpha^2},$$

$$\theta = \frac{T - T_c}{T_h - T_c}, \quad Pr = \frac{\nu}{\alpha}, \quad Ra = \frac{g\beta(T_h - T_c)L^3 Pr}{\nu^2}.$$

The above parameters lead to the following dimensionless governing equations

$$\frac{\partial U}{\partial X} + \frac{\partial V}{\partial Y} = 0, \tag{3.8}$$

$$U\frac{\partial U}{\partial X} + V\frac{\partial U}{\partial Y} = -\frac{\partial P}{\partial X} + Pr\left(\frac{\partial^2 U}{\partial X^2} + \frac{\partial^2 U}{\partial Y^2}\right) + RaPr\theta\sin\Phi, \tag{3.9}$$

$$U\frac{\partial V}{\partial X} + V\frac{\partial V}{\partial Y} = -\frac{\partial P}{\partial Y} + Pr\left(\frac{\partial^2 V}{\partial X^2} + \frac{\partial^2 V}{\partial Y^2}\right) + RaPr\theta\cos\Phi, \tag{3.10}$$

$$U\frac{\partial \theta}{\partial X} + V\frac{\partial \theta}{\partial Y} = \frac{\partial^2 \theta}{\partial X^2} + \frac{\partial^2 \theta}{\partial Y^2}. \tag{3.11}$$

The dimensionless boundary conditions on each wall of the cavity for the velocity and temperature fields are given by

- On the horizontal walls AB and CD:

$$U(X,Y) = 0, \quad V(X,Y) = 0, \quad \frac{\partial \theta}{\partial \mathbf{n}} = 0 \tag{3.12}$$

- On the right wall BC:

$$U(X,Y) = 0, \quad V(X,Y) = 0, \quad \theta = 0 \tag{3.13}$$

- On the left wall DA:

$$U(X,Y) = 0, \quad V(X,Y) = 0, \quad \theta = 1 \tag{3.14}$$

where **n** denotes the normal vector to the corressponding boundary component.

3.2 Numerical Procedure

For the solution, the non-dimensional governing Eqs. (3.8)-(3.11) with the boundary conditions (3.19)-(3.21) have been carried out numerically by finite element formulation based on the Galerkin weighted residual technique by using the bi-quadratic element for velocities (U, V) and temperature (θ), and discontinuous P_1 element for pressure [31].

Strong Form of Governing Equations:

$$\frac{\partial U}{\partial X} + \frac{\partial V}{\partial Y} = 0, \tag{3.15}$$

$$U\frac{\partial U}{\partial X} + V\frac{\partial U}{\partial Y} = -\frac{\partial P}{\partial X} + Pr\left(\frac{\partial^2 U}{\partial X^2} + \frac{\partial^2 U}{\partial Y^2}\right) + RaPr\theta\sin\Phi, \tag{3.16}$$

$$U\frac{\partial V}{\partial X} + V\frac{\partial V}{\partial Y} = -\frac{\partial P}{\partial Y} + Pr\left(\frac{\partial^2 V}{\partial X^2} + \frac{\partial^2 V}{\partial Y^2}\right) + RaPr\theta\cos\Phi, \tag{3.17}$$

$$U\frac{\partial \theta}{\partial X} + V\frac{\partial \theta}{\partial Y} = \frac{\partial^2 \theta}{\partial X^2} + \frac{\partial^2 \theta}{\partial Y^2}. \tag{3.18}$$

The Boundary Conditions:

- On the horizontal walls AB and CD:

$$U(X,Y) = 0, \quad V(X,Y) = 0, \quad \frac{\partial \theta}{\partial \mathbf{n}} = 0 \tag{3.19}$$

- On the right wall BC:

$$U(X,Y) = 0, \quad V(X,Y) = 0, \quad \theta = 0 \tag{3.20}$$

- On the left wall DA:

$$U(X, Y) = 0, \quad V(X, Y) = 0, \quad \theta = 1 \tag{3.21}$$

where **n** denotes the normal vector to the corresponding boundary component.

3.2.1 Weak Formulation/Variational Form

Variational formulation method/multiplier method or weak form is an approch in which governing equations (strong form) are transform into integral equations (weak form) by multiplying governing equations with suitable test function and integrated over the whole domain (Ω). In this section, Eqs. (3.15)-(3.18) together with the boundary conditions (3.19)-(3.21) illustrate to weaker form. First we multiply both sides of momentum equations and the temperature equation by test function $w \in \mathbf{W}$ and the continuity equation is multiplied by test function $q \in Q$ and then integrate over the whole domain where $\mathbf{W}$ and Q are test spaces. The test space $\mathbf{W} = (H^1(\Omega), H^1(\Omega), H^1(\Omega))$ is considered for the velocity components and temperature, and $Q = L^2(\Omega)$ is the test space for the pressure component. Thus, the variational/weak formulation of Eqs. (3.15)-(3.18) reads as follows:
Find $(U, V, \theta, P) \in \mathbf{W} \times Q$ such that

$$\int_{\Omega} \left(U \frac{\partial U}{\partial X} + V \frac{\partial U}{\partial Y} \right) w d\Omega - Pr \int_{\Omega} \left(\frac{\partial^2 U}{\partial X^2} + \frac{\partial^2 U}{\partial Y^2} \right) w d\Omega$$
$$- RaPr \sin \Phi \int_{\Omega} \theta w d\Omega + \int_{\Omega} \frac{\partial P}{\partial X} w d\Omega = 0, \tag{3.22}$$

$$\int_{\Omega} \left(U \frac{\partial V}{\partial X} + V \frac{\partial V}{\partial Y} \right) w d\Omega - Pr \int_{\Omega} \left(\frac{\partial^2 V}{\partial X^2} + \frac{\partial^2 V}{\partial Y^2} \right) w d\Omega$$
$$- RaPr \cos \Phi \int_{\Omega} \theta w d\Omega + \int_{\Omega} \frac{\partial P}{\partial Y} w d\Omega = 0, \tag{3.23}$$

$$\int_\Omega \left(\frac{\partial U}{\partial X} + \frac{\partial V}{\partial Y} \right) q d\Omega = 0, \tag{3.24}$$

$$\int_\Omega \left(U \frac{\partial \theta}{\partial X} + V \frac{\partial \theta}{\partial Y} \right) w d\Omega - \int_\Omega \left(\frac{\partial^2 \theta}{\partial X^2} + \frac{\partial^2 \theta}{\partial Y^2} \right) w d\Omega = 0. \tag{3.25}$$

for all $(w, q) \ \epsilon \mathbf{W} \times Q$.

In the Galerkin discretization, the infinite dimensional test and trial spaces are approximated by finite dimensional spaces. In particular, following are the trial and test spaces

Trial Spaces:

$\mathbf{U} \approx \mathbf{U_h}, \quad \mathbf{V} \approx \mathbf{V_h}, \quad \boldsymbol{\theta} \approx \boldsymbol{\theta_h} \quad \text{and} \quad P \approx P_h.$

Test Spaces:

$\mathbf{W} \approx \mathbf{W_h}, \quad Q \approx Q_h.$

The Galerkin discretization results into following non-linear discretized integral equations

$$Pr \int_\Omega \left(\frac{\partial U_h}{\partial X} \frac{\partial w_h}{\partial X} + \frac{\partial U_h}{\partial Y} \frac{\partial w_h}{\partial Y} \right) d\Omega + \int_\Omega \left(U_h \frac{\partial U_h}{\partial X} + V_h \frac{\partial U_h}{\partial Y} \right) w_h d\Omega$$
$$- RaPr \sin \Phi \int_\Omega \theta_h w_h d\Omega + \int_\Omega \frac{\partial P_h}{\partial X} w_h d\Omega = 0, \tag{3.26}$$

$$Pr \int_\Omega \left(\frac{\partial V_h}{\partial X} \frac{\partial w_h}{\partial X} + \frac{\partial V_h}{\partial Y} \frac{\partial w_h}{\partial Y} \right) d\Omega + \int_\Omega \left(U_h \frac{\partial V_h}{\partial X} + V_h \frac{\partial V_h}{\partial Y} \right) w_h d\Omega$$
$$- RaPr \cos \Phi \int_\Omega \theta_h w_h d\Omega + \int_\Omega \frac{\partial P_h}{\partial Y} w_h d\Omega = 0, \tag{3.27}$$

$$\int_\Omega \left(\frac{\partial U_h}{\partial X} + \frac{\partial V_h}{\partial Y} \right) q_h d\Omega = 0, \tag{3.28}$$

$$\int_\Omega \left(\frac{\partial \theta_h}{\partial X} \frac{\partial w_h}{\partial X} + \frac{\partial \theta_h}{\partial Y} \frac{\partial w_h}{\partial Y} \right) d\Omega + \int_\Omega \left(U_h \frac{\partial \theta_h}{\partial X} + V_h \frac{\partial \theta_h}{\partial Y} \right) w_h d\Omega = 0. \tag{3.29}$$

In the next step, discretized test and trial functions are approximated by using

finite element approximations. Thus, the above system of discrete integral equations lead to the following block matrix

$$
\underbrace{\begin{bmatrix} Pr\ L + N(\underline{U}, \underline{V}) & 0 & B_1 & -RaPr\sin\Phi\ M \\ 0 & Pr\ L + N(\underline{U}, \underline{V}) & B_2 & -RaPr\cos\Phi\ M \\ B_1^T & B_2^T & 0 & 0 \\ 0 & 0 & 0 & L + N(\underline{U}, \underline{V}) \end{bmatrix}}_{\mathbf{A}} \underbrace{\begin{bmatrix} \underline{U} \\ \underline{V} \\ \underline{P} \\ \underline{\theta} \end{bmatrix}}_{\mathbf{U}} = \underbrace{\begin{bmatrix} \underline{F}_1 \\ \underline{F}_2 \\ \underline{F}_3 \\ \underline{F}_4 \end{bmatrix}}_{\mathbf{F}}
$$

$$(3.30)$$

where,

$$
U_h = \sum_{j=1}^{NN} U_j\ \phi_j(x,y), \quad V_h = \sum_{j=1}^{NN} V_j\ \phi_j(x,y), \theta_h = \sum_{j=1}^{NN} \theta_j\ \phi_j(x,y),
$$

$$
P_h = \sum_{k=1}^{MN} P_k\ S_k(x,y),
$$

$\mathbf{A}$ is known as "block matrix", $\mathbf{U}$ is called "solution vector" and $\mathbf{F}$ is expressed as "load vector", the corresponding R.H.S after the implimentaion of boundary conditions. In the block matrix (3.30), L is the Laplace marix, M is mass matrix and N is the convective matrix. B_1 and B_2 are the pressure matrices, B_1^T, B_2^T are their corresponding transpose matrices and ϕ_j, S_k are shape function corresponding to spaces $(H^1(\Omega))$ and $(L^2(\Omega))$. By using the bi-quadratic Q_2-element of 3rd order accuracy the velocity components and temperature are discretized and pressure is approximated by P_1^{disc}-element of 2nd order accuracy (see [31] for details). The coupled non-linear equation are linearized by the Picard iteration method and the Guassian elimination method is utilized to solve the associated linear subproblems. Some tolerance value for the convergence of iterative scheme is prescribed to see the absolute difference of the two consecutive iteration values to the preceding iteration values. The stopping criterion to the iterative scheme is given by

$$
\left| \frac{\Upsilon^{n+1} - \Upsilon^n}{\Upsilon^{n+1}} \right| \le 10^{-6}, \tag{3.31}
$$

where n denotes the iteration number and Υ is used as variable to represent U, V, P, θ .

3.3 Code Validation

In order to validate the code adopted for the numerical solution of equations governing the natural convective flow, the comparison of current results with some of the earlier published work on free convection [1–4] are displayed in Table 3.1. Results obtained from the our code are in good agreement with the published results [1–4].

TABLE 3.1: Validation of the current code results with some published results of Refs. [1–4].

Ra	Present study	Ref. [1]	Ref. [2]	Ref. [3]	Ref. [4]
10^3	1.116	1.118	1.117	1.115	1.121
10^4	2.246	2.243	2.246	2.226	2.286
10^5	4.520	4.519	4.518	4.508	4.546

3.4 Results and Discussion

Galerkin weighted residual method is utilized to solve the equations governing the heat transfer and fluid flow. The obtained numerical results are visualized by means of streamlines and isotherms in the square inclined cavity which can be seen through Figures 3.2-3.4. The cavity for the given problem is considered with two walls (AB and CD) adiabatic walls, where the wall AD is kept at maximum temperature and the wall BC is kept cold. Effect of governing parameters on the flow such as Prandtl number, Rayleigh number and inclination angle for various considered values is observed.

Figure 3.2(a)-(d) illustrates the variation of the inclination angles ($\Phi = 15°$, $30°$ $60°$ and $75°$) on fluid flow in an inclined cavity with $Ra = 10^3$ and $Pr = 0.025$. At

$Ra = 10^3$, the isotherms are found to be slightly curved nature due to inclination angle effect. For all inclination angles, the isotherms are flattened near the top section of wall BC (cold wall) and lower section of wall DA (hot wall). Flow of the fluid inside square cavity is weak which can be viewed by low intensity of streamlines. The flow strength with augmentation in inclination angle decreases at low Rayleigh number as $|\psi|_{max} = 1.16, 1.16, 0.85$ and 0.50 for $\Phi = 15°, 30°, 60°$ and $75°$, respectively. The flow strength increases with the increment in Rayleigh number due to onset of convection. For $Ra = 10^4$ with $Pr = 0.025$, the isotherms in core of the enclosure are gradually contorted for all inclination angles. The convection starts gradually inside the cavity for $Ra = 10^4$.

Figure 3.3(a)-(d) depicts the fluid flow for $Ra = 10^5$ and $Pr = 0.025$ inside the cavity with varying inclination angles. The buoyancy driven forces with the Rayleigh number increases and thus convection at high Ra ($Ra = 10^5$) dominates in the enclosure. At $Ra = 10^5$, it is observed that the isotherms are extremely distorted for all inclination angles at the middle section of cavity due to dominance of convection. In contrast to previous case ($Ra = 10^3$), the isotherms for all Φ are found to be closed at top of wall BC (cold wall) and at the bottom of left wall DA (hot wall). The streamlines contours follow the similar circular pattern as in the previous case ($Ra = 10^3$). The flow intensity inside the cavity increases, irrespective of Φ which can be visualized by maximum magnitude of streamlines. The values of $|\psi|_{max}$ at $Ra = 10^5$ are 7.37, 8.47, 9.86 and 10.17 for $\Phi = 15°, 30°, 60°$ and $75°$, respectively (see Figure 3.3(a)-(d)).

Figure 3.4(a)-(d) illustrates the variation of inclination angles on isotherms and streamlines at $Ra = 10^5$ and $Pr = 998$. It is noticed that the isotherms at the lower section of wall DA and at the upper section of cold wall BC are highly compressed for all value of inclination angle Φ. It may be seen that the streamline contours occur in shape of enclosure near the walls, which contrasts the previous case with $Ra = 10^3$ where it was observed in circular pattern. The streamlines at the center of the cavity occur in almost elliptical shape for $\Phi = 30° 60°$ and $75°$, whereas almost dumbbell shape is observed in streamlines at $\Phi = 15°$. The maximum magnitude of streamlines indicates that the fluid flow intensity inside

the cavity is high compared to case ($Pr = 0.025$) for all values of Φ. At high Prandtl number ($Pr = 998$), the values observed for $|\psi|_{max}$ are 14.35, 17.53, 23.49 and 24.85 for $\Phi = 15°$, $30°$, $60°$ and $75°$, respectively.

The influence of the physical parameters i.e., $Ra = 10^3$ and Pr ($Pr = 0.025$ and 998) with varying inclination angle Φ on heat transfer is illustrated in Figure 3.5. For low Rayleigh number ($Ra = 10^3$), the declination in the graph of average Nusselt number has been observed for all inclination angles.

In Figure 3.6, the average heat transfer against the inclination angle Φ and physical parameters i.e., Rayleigh ($Ra = 10^5$) and Prandtl number ($Pr = 0.025$ and 998) is plotted. At $Pr = 0.025$, the enhancement in Nu_{avg} number has been observed for $\Phi = 15°$ - $60°$ and it decreases for $\Phi = 75°$. For the case of high Prandtl number, the rate of heat transfer enhanced for small inclination angles whereas the opposite effect has been observed for the large values of Φ.

The influence of Ra on heat transfer rate is depicted in Figure 3.7. The augmentation in the Nu_{avg} number is observed for both cases of Prandtl number. Maximum values of heat transfer rate are found at high Ra (i.e. $Ra = 10^5$) due to strong convection.
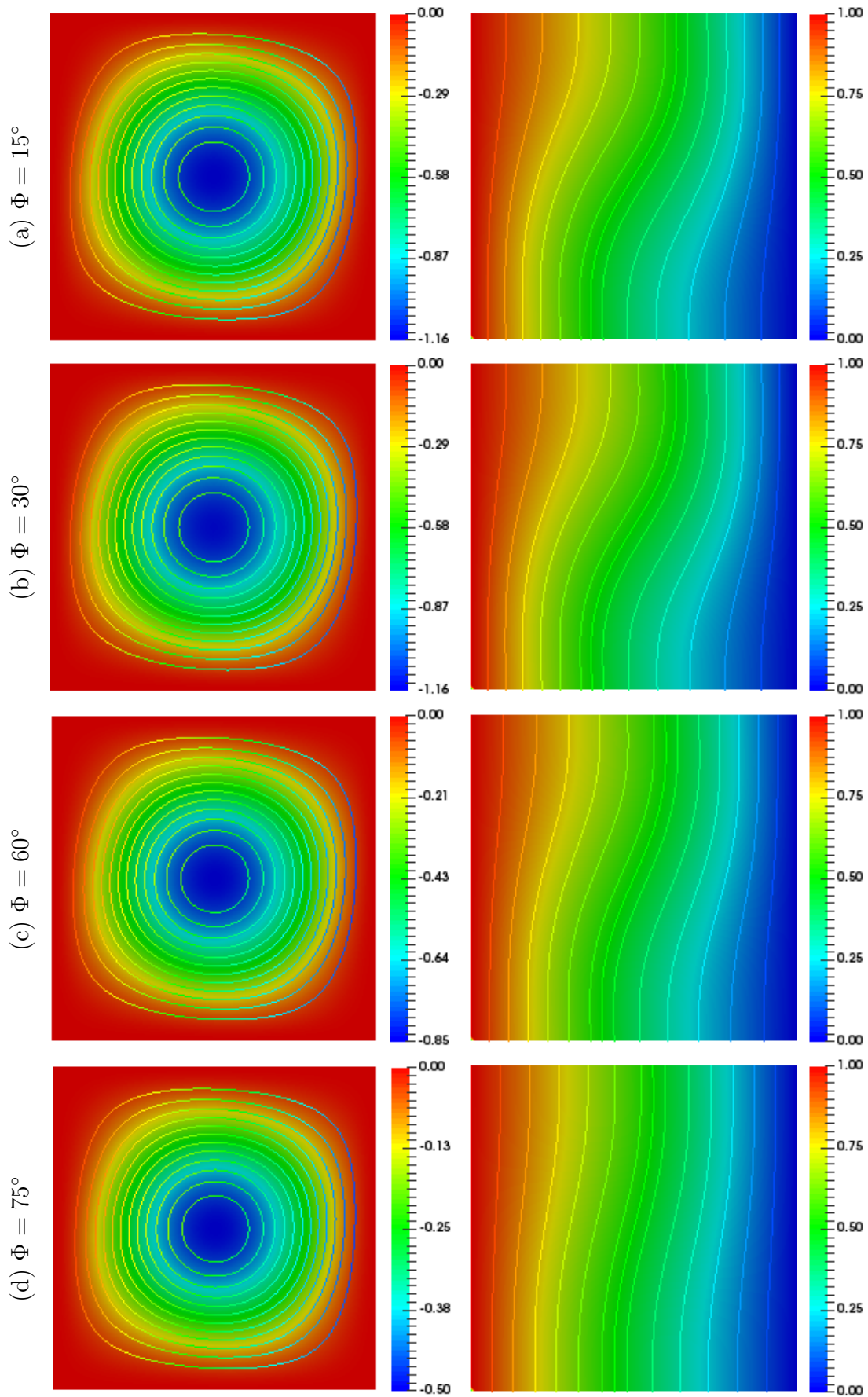
FIGURE 3.2: Streamlines (left) and isotherms (right) contours for different inclination angles (Φ) with $Ra = 10^3$ and $Pr = 0.025$.
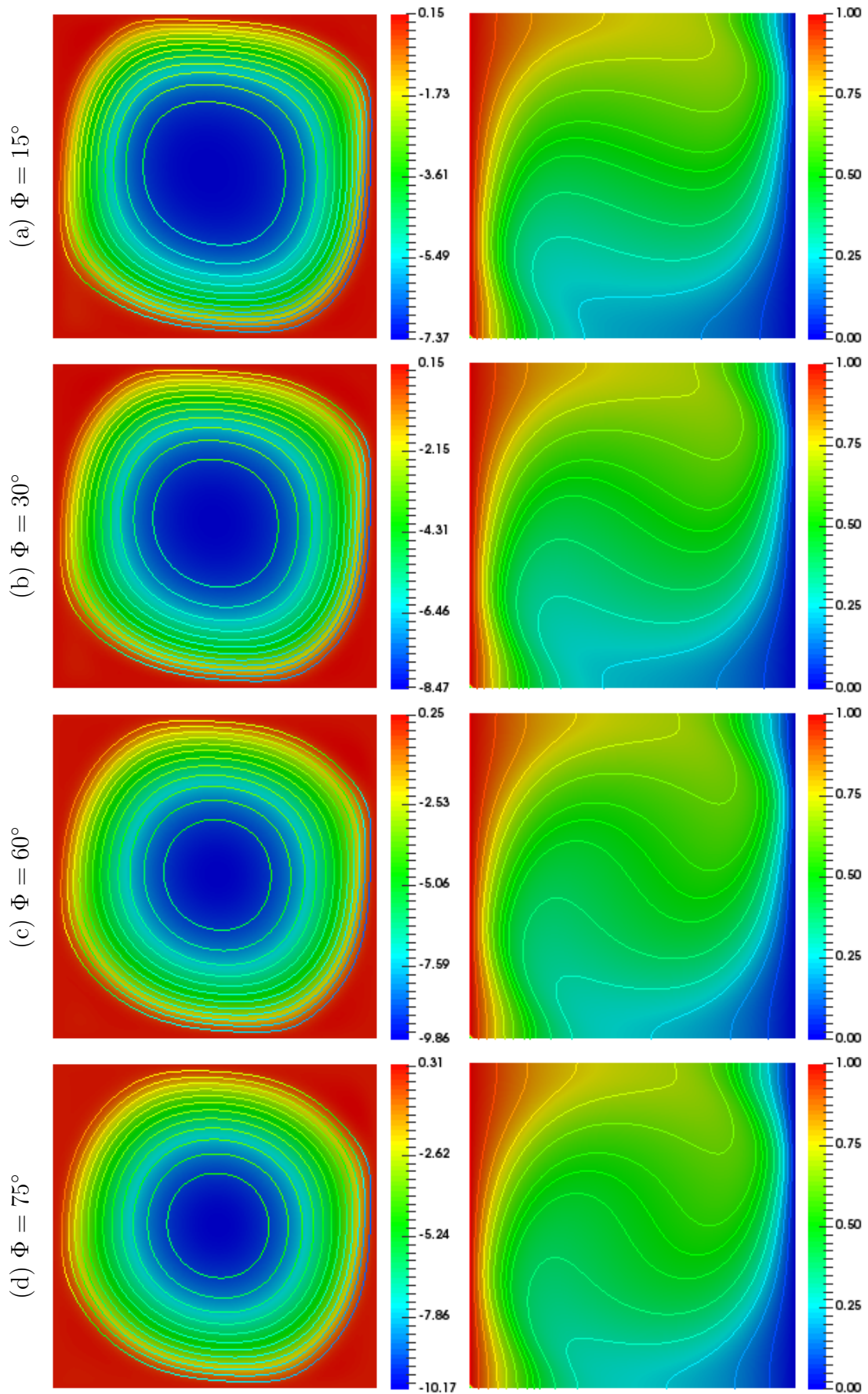
FIGURE 3.3: Streamlines (left) and isotherms (right) contours for different inclination angles with $Ra = 10^5$ and $Pr = 0.025$.
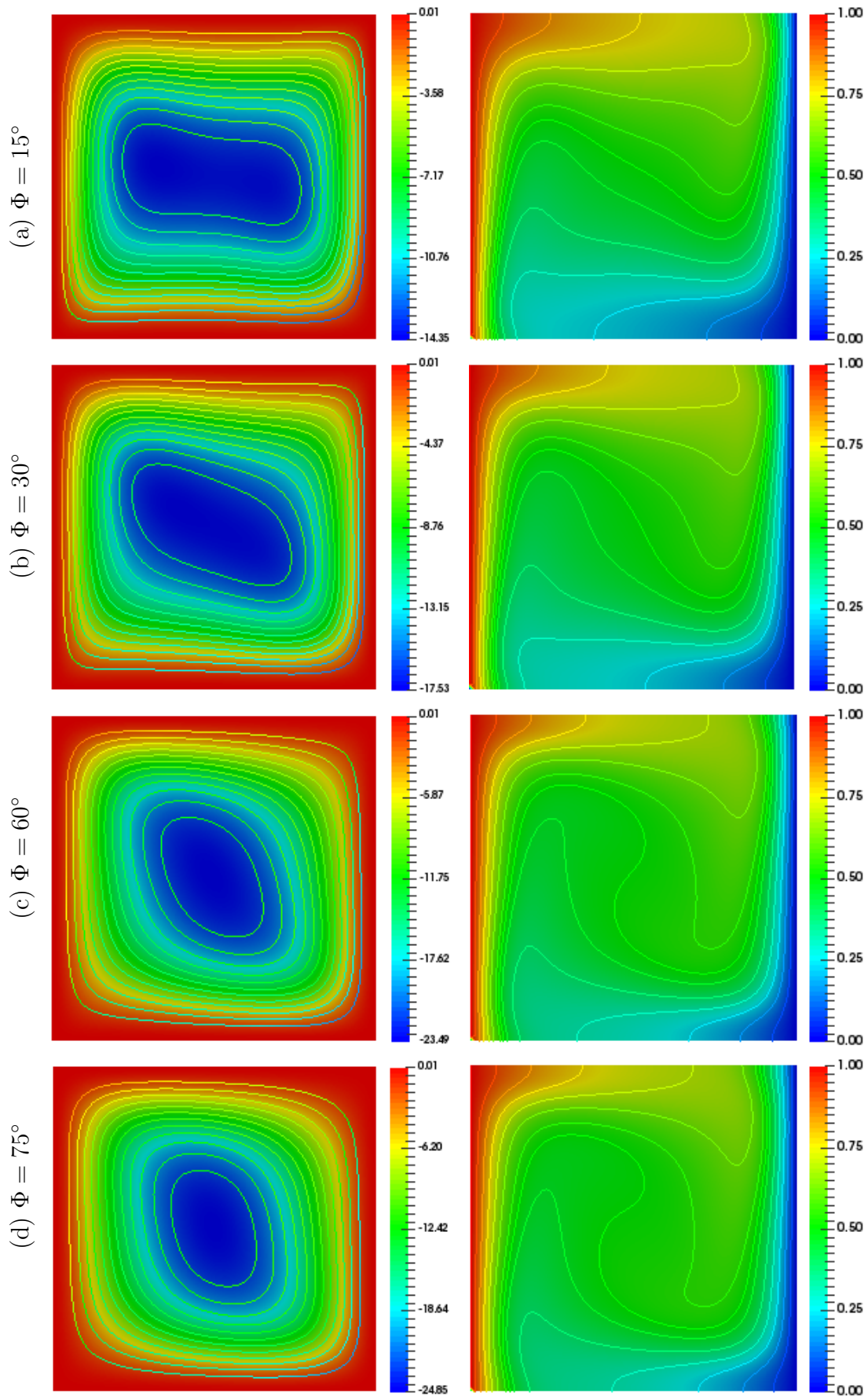
FIGURE 3.4: Streamlines (left) and isotherms (right) contours for different inclination angles with $Ra = 10^5$ and $Pr = 998$.
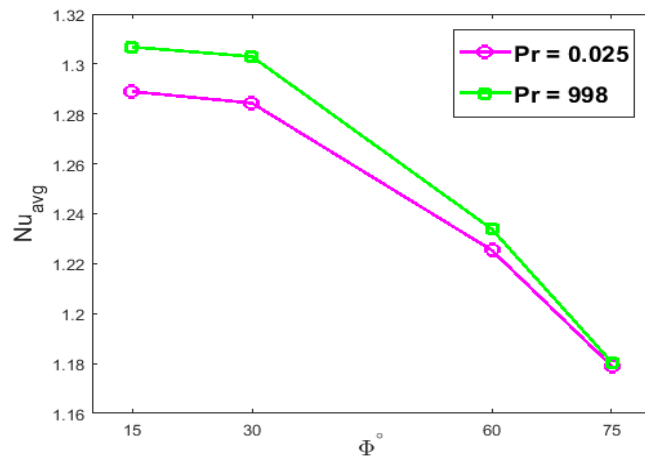
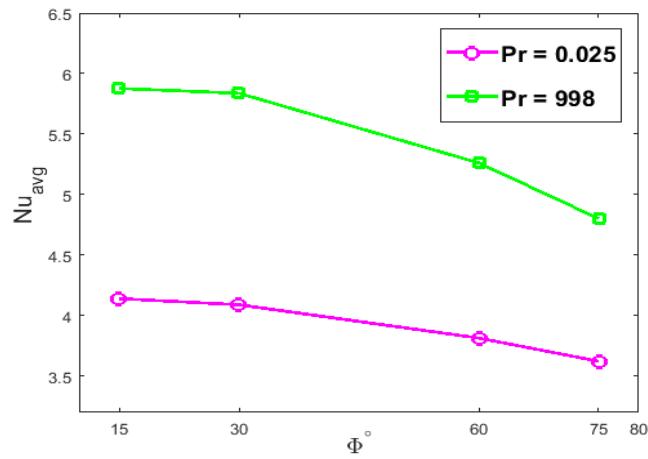FIGURE 3.5: Impact of Φ on Nu_{avg} number w.r.t Pr at fix $Ra = 10^3$.

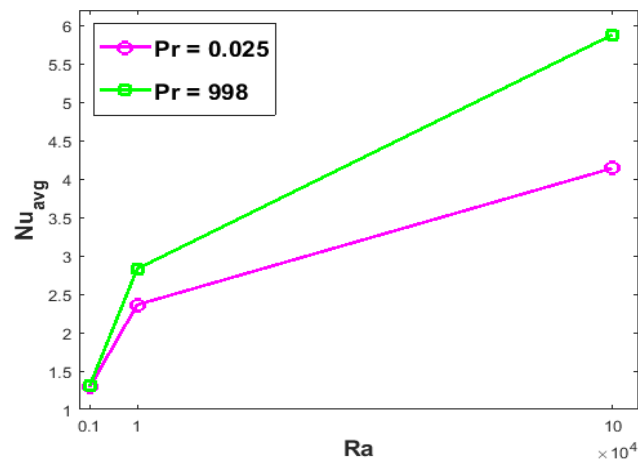FIGURE 3.6: Impact of Φ on Nu_{avg} number w.r.t Pr at fix $Ra = 10^5$.

FIGURE 3.7: Impact of Ra number on Nu_{avg} number w.r.t Pr at fix $\Phi = 15°$.

Chapter 4

Simulations of Natural Convective Flow in a Square Cavity with Non-linear Thermal Radiation

Based on the literature, in spite of the different studies have been considered on natural convection, there is a definite dearth of information regarding the natural convection flow in inclined square cavities with thermal radiation effect. The aim of the present work is to perform a numerical simulation of a two dimensional laminar free convective flow in an inclined square cavity with non-linear thermal radiation. In this chapter, we numerically find the solution for the steady and incompressible natural convective flow in a square tilted cavity. By means of an appropriate transformation, the governing equations are transformed into dimensionless coupled **PDEs** and they have been solved with the same procedure as in Chapter 3. The influence of governing parameters is analyzed through streamlines, isotherms and graphs. This work is an extension of the work presented in Chapter 3.

4.1 Problem Description and Mathematical Formulation

Let us take a two-dimensional, steady and incompressible natural convective flow in a tilted square cavity. The schematic diagram of the problem under consideration with boundary conditions as shown in Figure 3.1. The cavity is tilted at an inclination angle Φ with horizontal axis. Two parallel walls AB and CD of the cavity are assumed to be adiabatic where the wall BC is kept cold at temperature T_c (cold wall) and the wall DA of the enclosure is kept at high temperature T_h (hot wall). The enclosure is skewed at an angle Φ with horizontal axis. Under these assumptions, the equations of continuity, momentum and energy equation with non-linear thermal radiation takes the following form.

Continuity equation:

$$\frac{\partial u}{\partial x} + \frac{\partial v}{\partial y} = 0, \tag{4.1}$$

x-momentum equation:

$$u\frac{\partial u}{\partial x} + v\frac{\partial u}{\partial y} = -\frac{1}{\rho}\frac{\partial p}{\partial x} + \nu\left(\frac{\partial^2 u}{\partial x^2} + \frac{\partial^2 u}{\partial y^2}\right) + g\beta(T - T_c)\sin\Phi, \tag{4.2}$$

y-momentum equation:

$$u\frac{\partial v}{\partial x} + v\frac{\partial v}{\partial y} = -\frac{1}{\rho}\frac{\partial p}{\partial y} + \nu\left(\frac{\partial^2 v}{\partial x^2} + \frac{\partial^2 v}{\partial y^2}\right) + g\beta(T - T_c)\cos\Phi, \tag{4.3}$$

Energy equation:

$$u\frac{\partial T}{\partial x} + v\frac{\partial T}{\partial y} = \alpha\left(\frac{\partial^2 T}{\partial x^2} + \frac{\partial^2 T}{\partial y^2}\right) - C_1\left(\frac{\partial q_{rx}}{\partial x} + \frac{\partial q_{ry}}{\partial y}\right). \tag{4.4}$$

Here ν represent the kinematic fluid viscosity, ρ is fluid density, α is the thermal

diffusivity, the expansion coefficient is β, Φ is an inclination angle, fluid temperature is T, T_c is the cold right wall temperature, acceleration due to gravity is g, p is pressure of the fluid, $C_1 = \frac{1}{\rho c_p}$ and u, v denote the components of velocity.

The dimensional boundary conditions on each wall of the cavity for velocity and temperature fields are given by

- On the horizontal walls AB and CD:

$$u(x,y) = 0, \quad v(x,y) = 0, \quad \frac{\partial T}{\partial \mathbf{n}} = 0 \qquad (4.5)$$

- On the right wall CB:

$$u(x,y) = 0, \quad v(x,y) = 0, \quad T = T_c \qquad (4.6)$$

- On the left wall AD:

$$u(x,y) = 0, \quad v(x,y) = 0, \quad T = T_h \qquad (4.7)$$

where $\mathbf{n}$ denote the normal vector.

4.1.1 Dimensionless Form of the Governing Equations

The dimensionless form of the Eqs. (4.1)-(4.4) may be obtained by using the following dimensionless parameters [14]

$$X = \tfrac{x}{L}, \qquad Y = \tfrac{y}{L}, \qquad U = \tfrac{uL}{\alpha}, \qquad V = \tfrac{vL}{\alpha}, \qquad P = \tfrac{pL^2}{\rho\alpha^2}, \qquad \theta = \tfrac{T-T_c}{T_h-T_c},$$

$$Pr = \tfrac{\nu}{\alpha}, \qquad Ra = \tfrac{g\beta(T_h-T_c)L^3 Pr}{\nu^2}, \qquad N_r = \tfrac{T_h}{T_c}, \qquad Rd = \tfrac{4\sigma_* T_c^3}{a_R \kappa}.$$

The above parameters leads to the following dimensionless governing equations,

$$\frac{\partial U}{\partial X} + \frac{\partial V}{\partial Y} = 0, \tag{4.8}$$

$$U\frac{\partial U}{\partial X} + V\frac{\partial U}{\partial Y} = -\frac{\partial P}{\partial X} + Pr\left(\frac{\partial^2 U}{\partial X^2} + \frac{\partial^2 U}{\partial Y^2}\right) + RaPr\theta\sin\Phi, \tag{4.9}$$

$$U\frac{\partial V}{\partial X} + V\frac{\partial V}{\partial Y} = -\frac{\partial P}{\partial Y} + Pr\left(\frac{\partial^2 V}{\partial X^2} + \frac{\partial^2 V}{\partial Y^2}\right) + RaPr\theta\cos\Phi, \tag{4.10}$$

$$U\frac{\partial \theta}{\partial X} + V\frac{\partial \theta}{\partial Y} = \frac{\partial}{\partial X}\left(\frac{\partial \theta}{\partial X}(1 + \frac{4C_1}{3}Rd(1 + (N_r - 1)\theta)^3)\right)$$
$$+ \frac{\partial}{\partial Y}\left(\frac{\partial \theta}{\partial Y}(1 + \frac{4C_1}{3}Rd(1 + (N_r - 1)\theta)^3)\right). \tag{4.11}$$

The dimensionless boundary conditions on each wall of the cavity for velocity and temperature fields are given by

- On the horizontal walls AB and CD:

$$U(X,Y) = 0, \quad V(X,Y) = 0, \quad \frac{\partial \theta}{\partial \mathbf{n}} = 0 \tag{4.12}$$

- On the right wall CB:

$$U(X,Y) = 0, \quad V(X,Y) = 0, \quad \theta = 0 \tag{4.13}$$

- On the left wall AD:

$$U(X,Y) = 0, \quad V(X,Y) = 0, \quad \theta = 1 \tag{4.14}$$

where $\mathbf{n}$ denote the normal vector.

4.2   Numerical Method of Solution

The non-dimensional governing Eqs. (4.15)-(4.18) together with the boundary conditions (4.19)-(4.21) have been carried out numerically by Galerkin finite element method using the bi-quadratic element Q_2 for velocity and temperature,

and discontinuous P_1 element for pressure. First, the weak formulation of the governing equations is derived and then the solution is approximated by using the Galerkin approximation method.

Strong Form of Governing Equations:

$$\frac{\partial U}{\partial X} + \frac{\partial V}{\partial Y} = 0, \tag{4.15}$$

$$U\frac{\partial U}{\partial X} + V\frac{\partial U}{\partial Y} = -\frac{\partial P}{\partial X} + Pr\left(\frac{\partial^2 U}{\partial X^2} + \frac{\partial^2 U}{\partial Y^2}\right) + RaPr\theta\sin\Phi, \tag{4.16}$$

$$U\frac{\partial V}{\partial X} + V\frac{\partial V}{\partial Y} = -\frac{\partial P}{\partial Y} + Pr\left(\frac{\partial^2 V}{\partial X^2} + \frac{\partial^2 V}{\partial Y^2}\right) + RaPr\theta\cos\Phi, \tag{4.17}$$

$$U\frac{\partial\theta}{\partial X} + V\frac{\partial\theta}{\partial Y} = \frac{\partial}{\partial X}\left(\frac{\partial\theta}{\partial X}(1 + \frac{4C_1}{3}Rd(1 + (N_r - 1)\theta)^3)\right)$$
$$+ \frac{\partial}{\partial Y}\left(\frac{\partial\theta}{\partial Y}(1 + \frac{4C_1}{3}Rd(1 + (N_r - 1)\theta)^3)\right). \tag{4.18}$$

The Boundary Conditions are:

- On the horizontal walls AB and CD:

$$U(X,Y) = 0, \quad V(X,Y) = 0, \quad \frac{\partial\theta}{\partial\mathbf{n}} = 0 \tag{4.19}$$

- On the right wall BC:

$$U(X,Y) = 0, \quad V(X,Y) = 0, \quad \theta = 0 \tag{4.20}$$

- On the left wall DA:

$$U(X,Y) = 0, \quad V(X,Y) = 0, \quad \theta = 1 \tag{4.21}$$

where $\mathbf{n}$ denote the normal vector.

Weak Formulation/Variational Form:

Finding a solution in strong form is not always possible and there may be no smooth solution to a particular problem. To overcome these type of problems, weak formulation is preferred to find approximate solution. The main concept of weak formulation is turn the governing equations into integral equations. For the deriavtion of weak form, first multiply both sides of momentum equations and the temperature equation by test function $w \in \mathbf{W}$ and continuity equation is multiplied by test function $q \in Q$ and then integrate over the whole domain. Where $\mathbf{W}$ for (U, V) velocities, temperature and Q for pressure are test spaces as we used in Chapter 3. Thus, the variational/weak formulation of Eqs. (4.15)-(4.18) reads as follows

Find $(U, V, \theta, P) \in \mathbf{W} \times Q$ such that

$$\int_{\Omega} \left(U \frac{\partial U}{\partial X} + V \frac{\partial U}{\partial Y} \right) w d\Omega - Pr \int_{\Omega} \left(\frac{\partial^2 U}{\partial X^2} + \frac{\partial^2 U}{\partial Y^2} \right) w d\Omega$$
$$- RaPr \sin \Phi \int_{\Omega} \theta w d\Omega + \int_{\Omega} \frac{\partial P}{\partial X} w d\Omega = 0, \tag{4.22}$$

$$\int_{\Omega} \left(U \frac{\partial V}{\partial X} + V \frac{\partial V}{\partial Y} \right) w d\Omega - Pr \int_{\Omega} \left(\frac{\partial^2 V}{\partial X^2} + \frac{\partial^2 V}{\partial Y^2} \right) w d\Omega$$
$$- RaPr \cos \Phi \int_{\Omega} \theta w d\Omega + \int_{\Omega} \frac{\partial P}{\partial Y} w d\Omega = 0, \tag{4.23}$$

$$\int_{\Omega} \left(\frac{\partial U}{\partial X} + \frac{\partial V}{\partial Y} \right) q d\Omega = 0, \tag{4.24}$$

$$\int_{\Omega} \left(U \frac{\partial \theta}{\partial X} + V \frac{\partial \theta}{\partial Y} \right) w d\Omega - \int_{\Omega} \frac{\partial}{\partial X} \left(\frac{\partial \theta}{\partial X} (1 + \frac{4C_1}{3} Rd(1 + (N_r - 1)\theta)^3) \right) w d\Omega$$
$$- \int_{\Omega} \frac{\partial}{\partial Y} \left(\frac{\partial \theta}{\partial Y} (1 + \frac{4C_1}{3} Rd(1 + (N_r - 1)\theta)^3) \right) w d\Omega = 0. \tag{4.25}$$

for all $(w, q) \ \epsilon \ \mathbf{W} \times Q$.

In Galerkin discretization, the infinite dimensional test and trial spaces are approximated by finite dimensional spaces. In particular, following are the trial and test spaces

Trial Spaces:

$\mathbf{U} \approx \mathbf{U_h}, \quad \mathbf{V} \approx \mathbf{V_h}, \quad \boldsymbol{\theta} \approx \boldsymbol{\theta_h} \quad \text{and} \quad P \approx P_h.$

Test Spaces:

$\mathbf{W} \approx \mathbf{W_h}, \quad Q \approx Q_h.$

The Galerkin discretization results into following non-linear discretized integral equations

$$Pr \int_\Omega \left(\frac{\partial U_h}{\partial X} \frac{\partial w_h}{\partial X} + \frac{\partial U_h}{\partial Y} \frac{\partial w_h}{\partial Y} \right) d\Omega + \int_\Omega \left(U_h \frac{\partial U_h}{\partial X} + V_h \frac{\partial U_h}{\partial Y} \right) w_h d\Omega$$
$$- RaPr \sin \Phi \int_\Omega \theta_h w_h d\Omega + \int_\Omega \frac{\partial P_h}{\partial X} w_h d\Omega = 0, \tag{4.26}$$

$$Pr \int_\Omega \left(\frac{\partial V_h}{\partial X} \frac{\partial w_h}{\partial X} + \frac{\partial V_h}{\partial Y} \frac{\partial w_h}{\partial Y} \right) d\Omega + \int_\Omega \left(U_h \frac{\partial V_h}{\partial X} + V_h \frac{\partial V_h}{\partial Y} \right) w_h d\Omega$$
$$- RaPr \cos \Phi \int_\Omega \theta_h w_h d\Omega + \int_\Omega \frac{\partial P_h}{\partial Y} w_h d\Omega = 0, \tag{4.27}$$

$$\int_\Omega \left(\frac{\partial U_h}{\partial X} + \frac{\partial V_h}{\partial Y} \right) q_h d\Omega = 0, \tag{4.28}$$

$$\int_\Omega \left(U_h \frac{\partial \theta_h}{\partial X} + V \frac{\partial \theta_h}{\partial Y} \right) w_h d\Omega - \int_\Omega \frac{\partial}{\partial X} \left(\frac{\partial \theta_h}{\partial X} (1 + \frac{4C_1}{3} Rd(1 + (N_r - 1)\theta_h)^3) \right) w_h d\Omega$$
$$- \int_\Omega \frac{\partial}{\partial Y} \left(\frac{\partial \theta_h}{\partial Y} (1 + \frac{4C_1}{3} Rd(1 + (N_r - 1)\theta_h)^3) \right) w_h d\Omega = 0. \tag{4.29}$$

In the next step, discretized test and trial functions are approximated by using finite element approximations. Solving the above system of discrete integral equations lead to the following block matrix

$$\underbrace{\begin{bmatrix} Pr\ L + N(\underline{U}, \underline{V}) & 0 & B_1 & -RaPr \sin \Phi\ M \\ 0 & Pr\ L + N(\underline{U}, \underline{V}) & B_2 & -RaPr \cos \Phi\ M \\ B_1^T & B_2^T & 0 & 0 \\ 0 & 0 & 0 & L + N(\underline{U}, \underline{V}) \end{bmatrix}}_{\mathbf{A}} \underbrace{\begin{bmatrix} \underline{U} \\ \underline{V} \\ \underline{P} \\ \underline{\theta} \end{bmatrix}}_{\mathbf{U}} = \underbrace{\begin{bmatrix} \underline{F}_1 \\ \underline{F}_2 \\ \underline{F}_3 \\ \underline{F}_4 \end{bmatrix}}_{\mathbf{F}}$$
$$\tag{4.30}$$

where,

$$U_h = \sum_{j=1}^{MM} U_j \ \phi_j(x,y), \quad V_h = \sum_{j=1}^{MM} V_j \ \phi_j(x,y), \quad \theta_h = \sum_{j=1}^{MM} \theta_j \ \phi_j(x,y),$$

$$P_h = \sum_{k=1}^{MN} P_k \ S_k(x,y),$$

In the block matrix (4.30), L is the Laplace marix, M is mass matrix and N is the convective matrix. B_1 and B_2 are the pressure matrices and B_1^T, B_2^T are their corresponding transpose matrices. Velocity components and temperature are discretized and pressure is approximated with the same element as in Chapter 3. The coupled non-linear equation are linearized by the Picard iteration method and Guassian elimination method is utilized to solve the associated linear subproblems. The stopping criterion to the iterative scheme is given by

$$\left| \frac{\Upsilon^{n+1} - \Upsilon^n}{\Upsilon^{n+1}} \right| \le 10^{-6}, \tag{4.31}$$

where n denotes the iteration number and Υ is used as variable to represent U, V, P, θ .

4.3   Results and Discussion

To study the thermal radiation effect on free convective heat transfer in inclined square cavity, application of FEM is performed to solve governing equations by applying the Galerkin finite element method. Under investigation of tilted cavity (see 3.1) with two horizontal walls (DC and AB) are assumed to be adiabatic in boundary condition and vertical walls with thermal boundary condition i.e; activation of temperature on left wall(AD) and right wall(CB) cold. Simulations are performed for two dimensional, steady and incompressible natural convective flow with thermal radiation and presented in term of streamlines (left) and isotherms (right) for different values of physical parameters. The governing parameters are Prandtl number ($Pr = 0.025$ for mercury, $Pr = 0.71$ for air, $Pr = 6.2$ for water,

$Pr = 998$ for glycerol), Rayleigh number ($Ra = 10^2, 10^3, 10^4, 10^5$), radiation parameter ($Rd = 0, 1, 2, 3$) with angle of inclination ($\Phi = 15°, 30°, 60°, 75°$). Discrete endeavour have been focused on the influence of these parameters. The strength of motion inside the cavity in term of local and Nu_{avg} number, numerical results are presented for the various values of key parameters.

Figure 4.1(a)-(d) illustrate the effect of Rayliegh number ($Ra = 10^2 - 10^5$) on streamlines and isotherms, while the other parameters kept fixed i.e., $Pr = 0.025$, $\Phi = 15°$ and $Rd = 1$. From Figure 4.1(a), it can be observe that the hot fluid rises to the wall DA of cavity due to the inclination effect of the enclosure. In this case, the transfer of heat is mainly due to conduction as the isotherm counters are uniformly distributed. It was examined that the concentration of streamlines is very low due to conduction dominant heat transfer. It can be investigated through Figure 4.1(b), with augmentation in the Ra causes a curvature in the isotherms. The isotherms are semi-parallel to walls BC and DA of the cavity. A moderate enhancement in the intensity of streamfunction is likewise investigated. The convection heat switch mode starts at $Ra = 10^4$ due to which disturbance inside the streamlines arise at the middle section of the enclosure. Further, augmented convection patterns arise within the cavity for high ($Ra = 10^5$) and high deformation in the isotherm contours arise at the middle section of cavity due to dominance of convection. Within the cavity, streamlines arise nearly in a circular shape in all cases. It is obvious from the maximum value of streamfuntion , the strength of fluid flow increased inside the cavity with growth in Ra (see Figure 4.1 (a)-(d)). For all cases taken under consideration the values observed for $|\psi|_{max}$ are 0.12, 1.17, 5.18 and 10.63 for $Ra = 10^2$, 10^3, 10^4, 10^5, respectively.

Influence of the various Pr ($Pr = 0.025$, 0.71, 6.2, 998) on streamlines and isotherms in square tilted enclosure with $\Phi = 15°$, $Rd = 1$ and $Ra = 10^4$, is displayed in Figure 4.2(a)-(d). With increase in prandtl number (Pr), the streamfunction rapidly grows in magnitude for low prandtl numbers ($Pr = 0.025$, 0.71)

due to which disturbance occurs at the middle section of cavity and slightly increases for high prandtl number ($Pr = 6.2,\ 998$) as $|\psi|_{max} = 5.18, 8.63, 8.76$ and 8.78, respectively. For all the Pr, the compression in isotherms near the top section of opposite wall CB and at the bottom section of wall AD is observed. The counters of isotherms follows almost the similar pattern for all values of prandtl number.

Effect of thermal radiation parameter ($Rd = 0 - 3$) on streamlines and isotherms distribution with $Pr = 0.025,\ \Phi = 15°$ and $Ra = 10^4$ is displayed in Figure 4.3(a)-(d). Irrespective of the various radiation parameters, a single cell forms within the cavity illustrating ascending flows closer to the hot vertical wall counters streamline and isotherm are uniformly distributed. That's why we can find rotation of fluid close to left wall DA intensive in magnitude. Furthermore, close the hot wall DA the cellular core arises due to convection at high temperature within the cavity. With the increase in (Rd) assists to an enhancement of convection phenomenon of heat transfer in addition to augmentation of heat conduction. At the centre of cavity the bending behaviour of isotherm as well as the layers of thermal boundary near to walls DA and BC reduces in (see in Figure 4.3 (c)-(d)). Under discussion the values observed for $|\psi|_{max}$ are 4.29, 5.18, 5.46 and 5.56.

Figure 4.4 depicts the fluid flow for $\Phi = 15°$, $Rd = 1$ and $Ra = 10^5$ inside the cavity with varying prandtl number ($Pr = 0.025,\ 0.71,\ 6.2,\ 998$) in term of streamlines and isotherms. It is examined that the concentration of isotherms near to hot wall DA increases which evident the increase in heat transfer (see in Figure 4.4 - (b)). Medium of inclined square enclosure is exchange by different material having high value of prandtl number, viscosity dominant effect can be seen in movement of streamline downward (Figure 4.4 (c)-(d)). With varying prandtl number(Pr), the streamfunction rapidly grows in magnitude for low prandtl numbers ($Pr = 0.025,\ 0.71$) due to which disturbance occurs at the middle section of cavity and slightly increases for high prandtl number ($Pr = 6.2,\ 998$) as $|\psi|_{max} = 10.63, 21.04, 23.53$ and 24.40, respectively. Figure 4.5(a)-(d) illustrates the fluid flow within the enclosure for $Pr = 0.025$, $Ra = 10^5$ and $Rd = 1$ with varying the impact of inclination angle. The buoyancy driven forces with the Rayleigh number increases

and thus convection at high Ra dominates in the enclosure. At $Ra = 10^5$, it is noticed that the isotherms are distorted for all inclination angles at the middle section of the cavity due to dominance of convection. In this case, the isotherms for all Φ are noticed to be closed near the top of wall BC (cold wall) and the bottom of left wall DA (hot wall). The streamlines contours follow the similar circular pattern. The flow intensity inside the cavity increases, irrespective of Φ which can be visualized by maximum magnitude of streamlines. The values of $|\psi|_{max}$ at $Ra = 10^5$ are 10.63, 21.04, 23.53 and 24.40 for $\Phi = 15°$, $30°$, $60°$ and $75°$, respectively (see Figure 4.5(a)-(d)).

Impact of thermal radiation parameter (Rd) on streamlines and isotherms distribution with $Pr = 0.025$, $\Phi = 15°$ and $Ra = 10^5$ is displayed in Figure 4.6(a)-(d). In contrast to case $(Ra = 10^4)$, the isotherms for all Rd are noticed to be closed near the top of wall BC (cold wall) and at the bottom of left wall DA (hot wall). Due to high Ra, buoyancy driven forces more effective with convection dominates in cavity as well as intensity of streamfunction also rises in contrast to previous case $(Ra = 10^4)$. That's why we can find rotation of fluid close to left wall DA more intensive in magnitude. The streamlines contours follow the similar circular pattern as in the previous case $(Ra = 10^4)$. With enhancement in Rd, the streamfunction grows in magnitude as $|\psi|_{max}$ at $Ra = 10^5$ are 7.37, 10.63, 12.13 and 12.96 for $Rd = 0, 1, 2, 3, 4$. For all Rd, a single cell forms within the cavity illustrating ascending flows close to the hot vertical wall counters streamline and isotherm are uniformly distributed. Influence of the various inclination angle ($\Phi = 15°$, $30°$ $60°$ and $75°$) on fluid flow in an inclined cavity with $Pr = 0.71$, $Rd = 1$ and $Ra = 10^3$ is displayed in term of streamlines and isotherms distribution (see Figure 4.7(a)-(d)). At $Ra = 10^3$, the isotherms are found to be slightly curved nature due to inclination angle effect($\Phi = 15°$, $30°$). For other inclination angles ($\Phi = 60°$, $75°$), the isotherms are flattened closevto the top section of wall BC (cold wall) and lower section of wall DA (hot wall). Due to increase in Pr the viscous effect is dominant that yields flow of the fluid inside square cavity is weaker which can be viewed by low intensity of streamlines. The flow strength with augmentation in

inclination angle decreases at low Rayleigh number as $|\psi|_{max} = 1.26, 1.19, 0.75$ and 0.40 for $\Phi = 15°, 30°, 60°$ and $75°$, respectively.

Figure 4.8(a)-(d) depicts the strong impact of Rayliegh number ($Ra = 10^2 - 10^5$) on streamlines and isotherms, while the other parameters kept fixed i.e., $Pr = 0.71$, $\Phi = 15°$ and $Rd = 1$. From Figure 4.8(a), it can be observe that the hot fluid rises to the wall DA of cavity due to the inclination effect of the enclosure. In this case, the transfer of heat is mainly due to conduction as the isotherm counters are uniformly distributed. It was examined that the concentration of streamlines is low due to the effect of conduction governing heat transfer. In contrast to previous case ($Pr = 0.025$), it can be investigated through Figure 4.8(b), with augmentation in the Ra causes a more inclination in the isotherms. The isotherms are semi-parallel to walls BC and DA of the enclosure. A compareable enhancement in the intensity of streamfunction is likewise noticed. The convection heat switch mode starts at $Ra = 10^4$ due to which disturbance inside the streamlines arises at the middle section of the enclosure. Further, enhanced convection patterns arise within the cavity for high ($Ra = 10^5$) and high deformation in the isotherm contours arise at the middle section of enclosure and thus convection dominates. Within the cavity, streamlines arise nearly in a circular shape in all cases. It is obvious from the maximum value of streamfuntion , the strength of fluid flow increased inside the cavity with growth in Ra (see in Figure 4.8 (a)-(d)). For all cases taken under consideration the values observed for $|\psi|_{max}$ are 0.12, 1.26, 8.63 and 21.04 for $Ra = 10^2, 10^3, 10^4, 10^5$, respectively.

Effect of thermal radiation parameter ($Rd = 0 - 4$) on streamlines and isotherms distribution with $Pr = 0.71$, $\Phi = 15°$ and $Ra = 10^4$ is displayed in Figure 4.9(a)-(d). We can find rotation of fluid close to left wall DA intensive in magnitude. Furthermore, close the hot wall DA the cellular core arises due to convection at high temperature witin the cavity. With the enhancement in radiation parameter assists to an augmentation of both convection phenomenon of heat transfer and heat conduction in addition to the attenuation of size of core of convection. At the centre of cavity the bending behaviour of isotherm as well as the layers of thermal

boundary near to walls DA and BC reduces in (see in Figure 4.9 (c)-(d)). Under discussion the values observed for $|\psi|_{max}$ are 6.03, 8.63, 10.06 and 10.92. For $Pr = 0.71$, $Rd = 1$ and $Ra = 10^5$,the Figure 4.10(a)-(d) illustrates the fluid flow inside the cavity with varying inclination angles(ϕ). The buoyancy driven forces with the Rayleigh number increases and thus convection at high Ra dominates in the cavity. At $Ra = 10^5$, it is investigated that the isotherms are distorted for all inclination angles at the middle section of the enclosure due to dominance of convection. In this case ($Ra = 10^5$), the isotherms for all Φ are observed to be compressed near the top of wall BC (cold wall) and the bottom of left wall DA (hot wall). The streamlines contours, follow the high distortion (see in Figure 4.10 (a)-(b)) while similar circular pattern (see in Figure 4.10 (c)-(d)). The flow intensity inside the cavity gradually increases, irrespective of Φ which can be visualized by maximum magnitude of streamlines. The values of $|\psi|_{max}$ at $Ra = 10^5$ are 21.04, 26.69, 34.85 and 36.43 for $\Phi = 15°$, $30°$, $60°$ and $75°$, respectively (see Figure 4.10(a)-(d))

Impact of thermal radiation parameter (Rd) on streamlines and isotherms distribution with $Pr = 0.71$, $\Phi = 15°$ and $Ra = 10^5$ is displayed in Figure 4.11(a)-(d). The isotherms for all Rd are noticed to be compressed close to the top of wall BC (cold wall) and the bottom of left wall DA (hot wall). Due to high $Ra = 10^5$, buoyancy driven forces more effective with high convection dominates in cavity as well as intensity of streamfunction also rapidly rises in contrast to previous case $(Ra = 10^4)$. The streamlines contours follow the distorted distribution for $Rd = 0, 1$ and similar circular pattern for $Rd = 2, 3$ as in the previous case $(Ra = 10^4)$. With enhancement in Rd, the streamfunction grows in magnitude as $|\psi|_{max}$ at $Ra = 10^5$ are 12.20, 21.04, 28.97 and 35.30 for $Rd = 0, 1, 2, 3, 4$.

Figure 4.12-4.20 dipicts the average Nusselt number (Nu_{avg}) distribution along the left wall DA for various values of Pr, Φ, Rd and Ra. The influence of prandtl on average Nusselt number can be visualized through Figure 4.12 for various cases of Ra. The average Nusselt number increases in significant behaviour by keeping the values of inclination angle and thermal radiation parameter fixed i.e., $\Phi = 15°$ and

$Rd = 1$. This is due to the fact that convection is dominant inside the enclosure resulting enhancement in the rate of heat transfer.

In Figure 4.13, the variation in inclination angle against average Nusselt number has been depicted w.r.t Rayleigh number. The average Nusselt number first increases for inclination angles $\Phi = 15°, 30°$ then a light decrease is observed for $\Phi = 60°$ and it further decreases for $\Phi = 75°$. The impact of non-linear thermal radiation parameter considering different cases of Ra for the heat transfer rate can be visualized through Figure 4.14. Values of inclination angle and thermal radiation parameter are kept fixed i.e., $\Phi = 15°$ and $Rd = 1$. The average Nusselt number first increases gradually for $Rd = 0, 1$ and it slightly increses for $Rd = 2, 3$. In Figure 4.15, the variation in inclination angle against average Nusselt number has been depicted w.r.t prandtl number. For fixed value of radiation parameter and Rayleigh number i.e., $Rd = 1$ and $Ra = 10^3$, the average Nusselt number first slightly decreases for $\Phi = 15°, 30°$ and decreases gradually for $\Phi = 60°, 75°$. In Figure 4.16, the variation in inclination angle against average Nusselt number has been depicted w.r.t prandtl number. For fixed value of radiation parameter and Rayleigh number i.e., $Rd = 1$ and $Ra = 10^4$, the average Nusselt number first increases for $\Phi = 15°, 30°$ and decreases slightly for $\Phi = 60°$ further gradually decreases for $75°$.

In Figure 4.17, the variation in inclination angle against average Nusselt number has been depicted w.r.t prandtl number. For fixed value of radiation parameter and Rayleigh number i.e., $Rd = 1$ and $Ra = 10^5$, the average Nusselt number first decreases slightly for $\Phi = 15°, 30°$ and further decreases for $\Phi = 60°, 75°$.

In Figure 4.18, shows the impact of radiation parameter on Nu_{avg} number for various cases of prandtl number. The Nu_{avg} number increases for fix value of inclination angle and Rayleigh number i.e., $\Phi = 15°$ and $Ra = 10^4$.

In Figure 4.19, shows the variation of Rd on Nu_{avg} number for various cases of prandtl number. The Nu_{avg} number increases for fix value of inclination angle and Rayleigh number i.e., $\Phi = 15°$ and $Ra = 10^5$.

The impact of Rayleigh number for different cases of prandtl parameter on the heat transfer rate can be visualized through Figure 4.20. Values of inclination angle and thermal radiation parameter are kept fixed i.e., $\Phi = 15°$ and $Rd = 1$. The increment in Nu_{avg} number is observed by increasing the Ra. This is due to the fact that convection is dominant inside the cavity for high Rayleigh numbers $(Ra \geq 10^4)$ resulting increase in the rate of heat transfer.
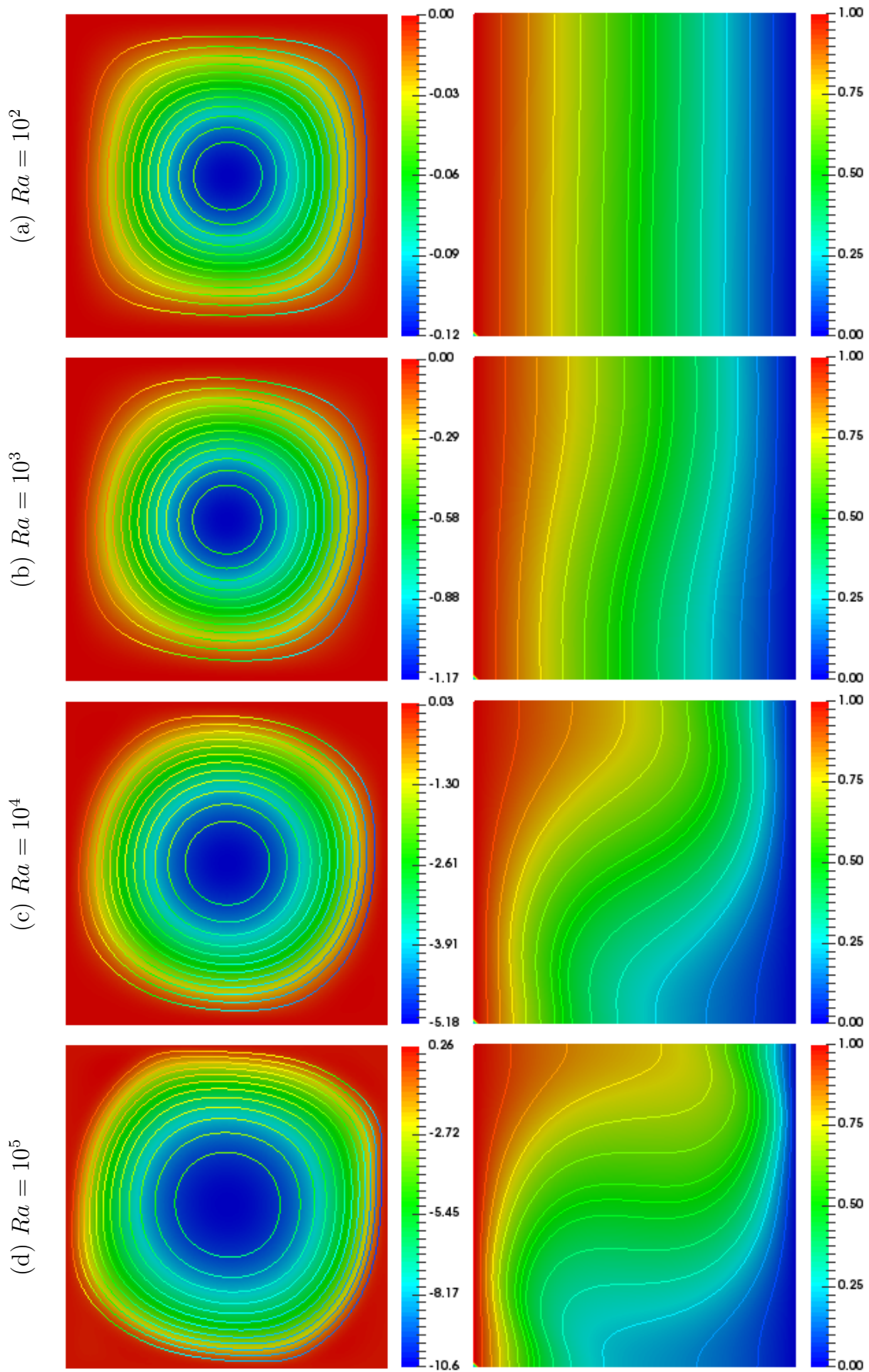
FIGURE 4.1: Influence of Rayleigh number $(Ra = 10^2 - 10^5)$ on streamlines (left) and isotherms (right) with parameters $Pr = 0.025$, $\Phi = 15°$, $Nr = 1.1$ and $Rd = 1$.
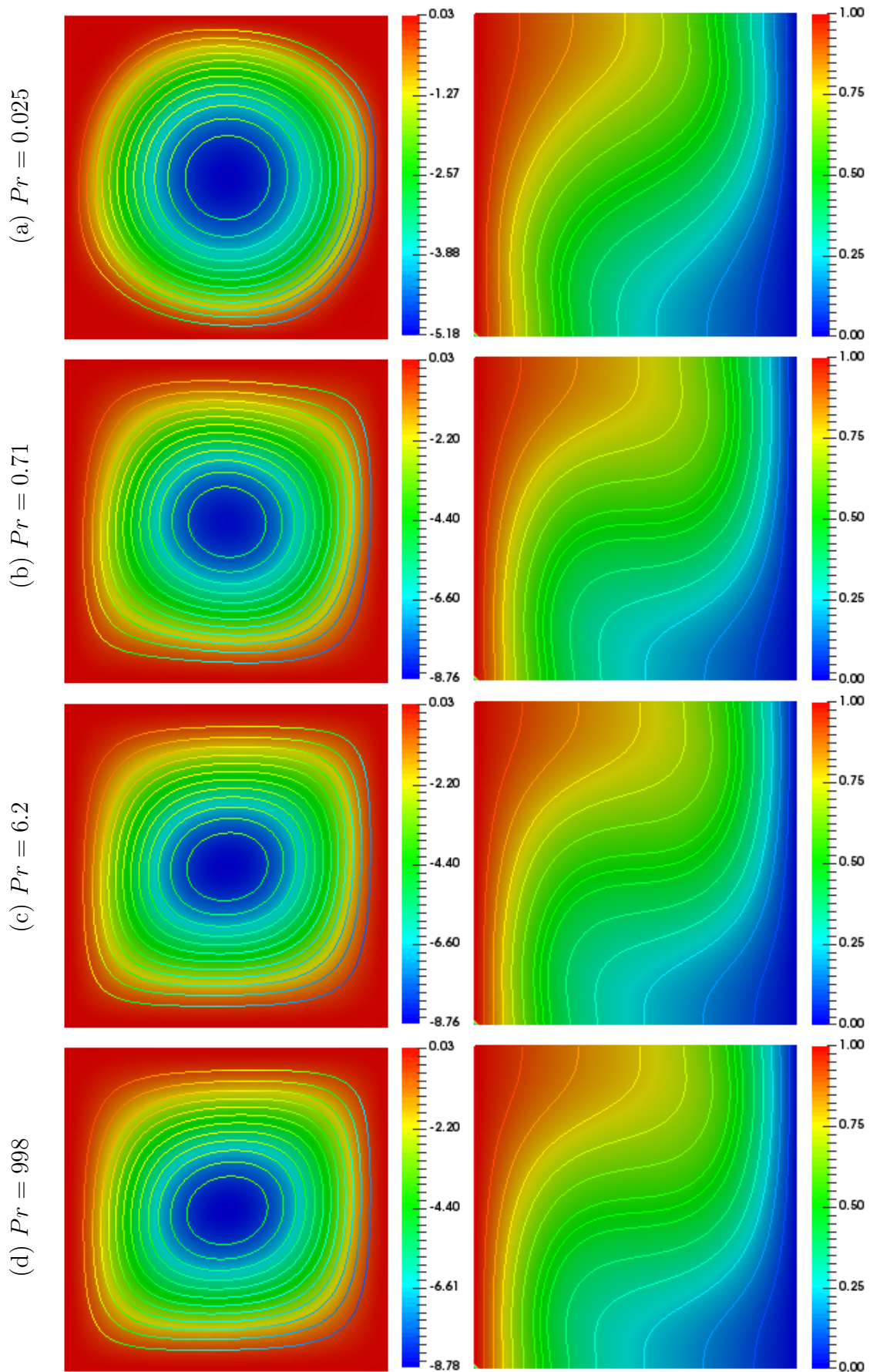
FIGURE 4.2: Impact of Pr on streamlines (left) and isotherms (right) at $\Phi = 15°$, $Nr = 1.1$, $Rd = 1$ and $Ra = 10^4$.
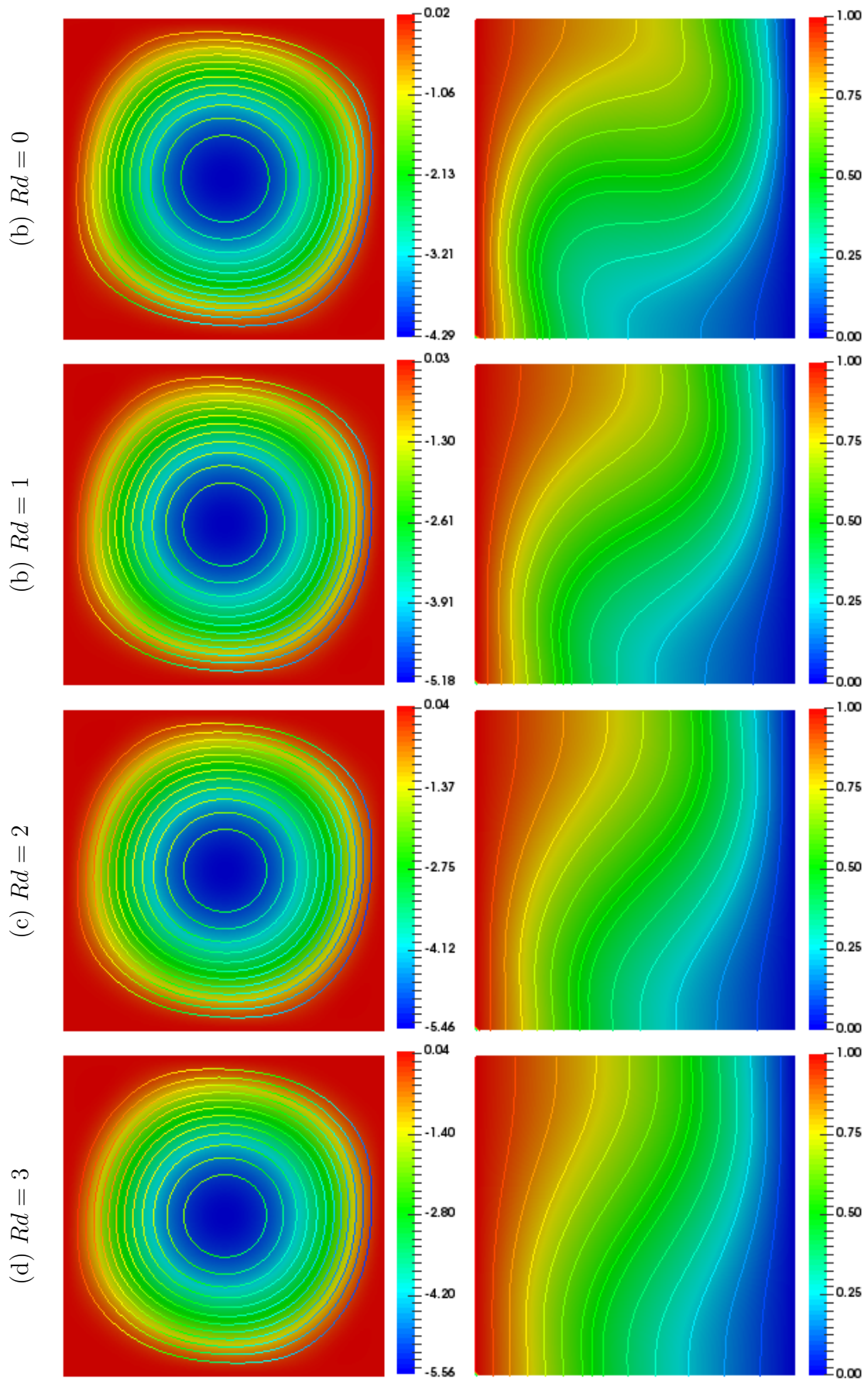
FIGURE 4.3: Impact of Radiation parameter (Rd) on streamlines (left) and isotherms (right) with $Pr = 0.025$, $\Phi = 15°$, $Nr = 1.1$ and $Ra = 10^4$.
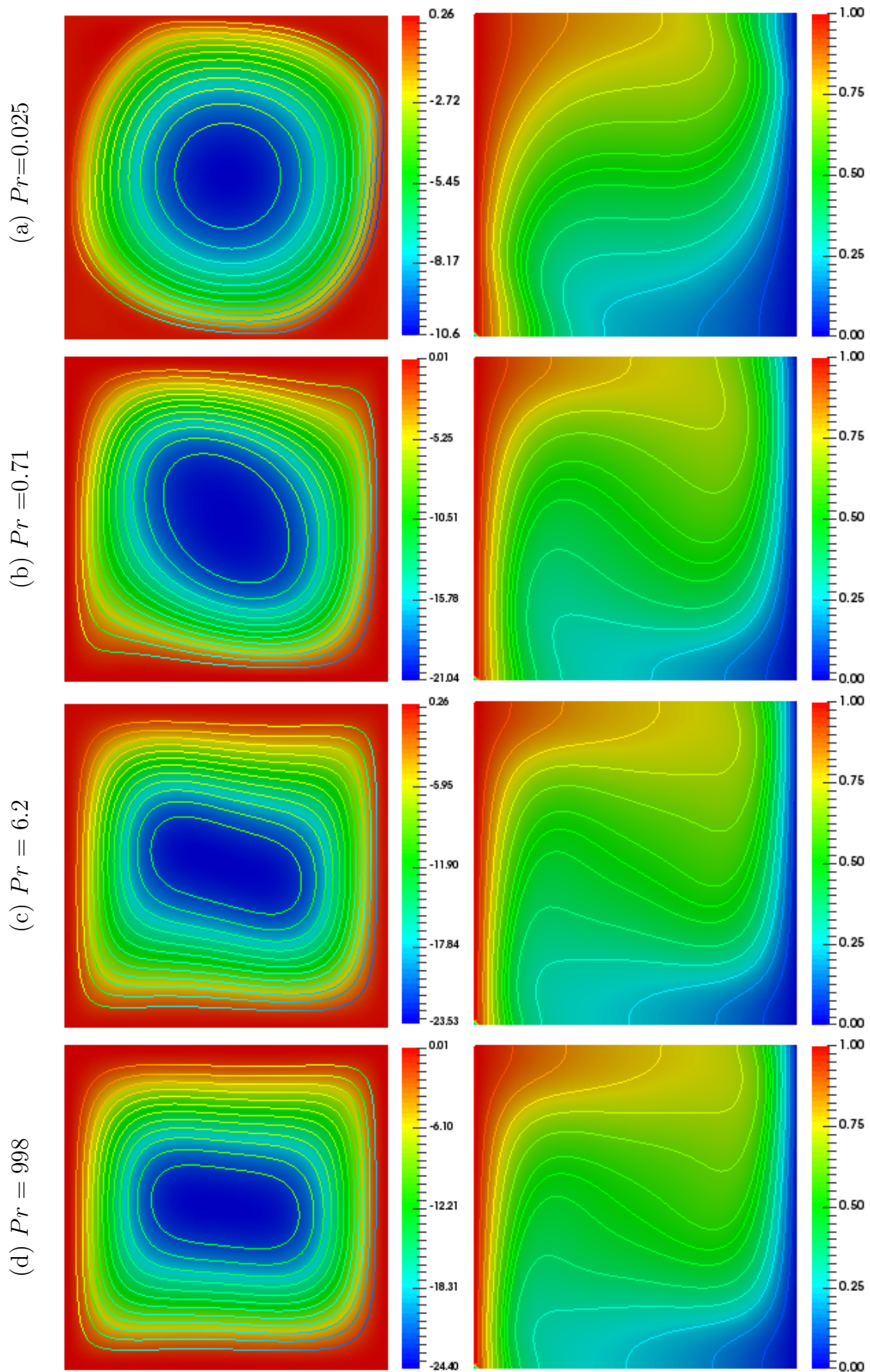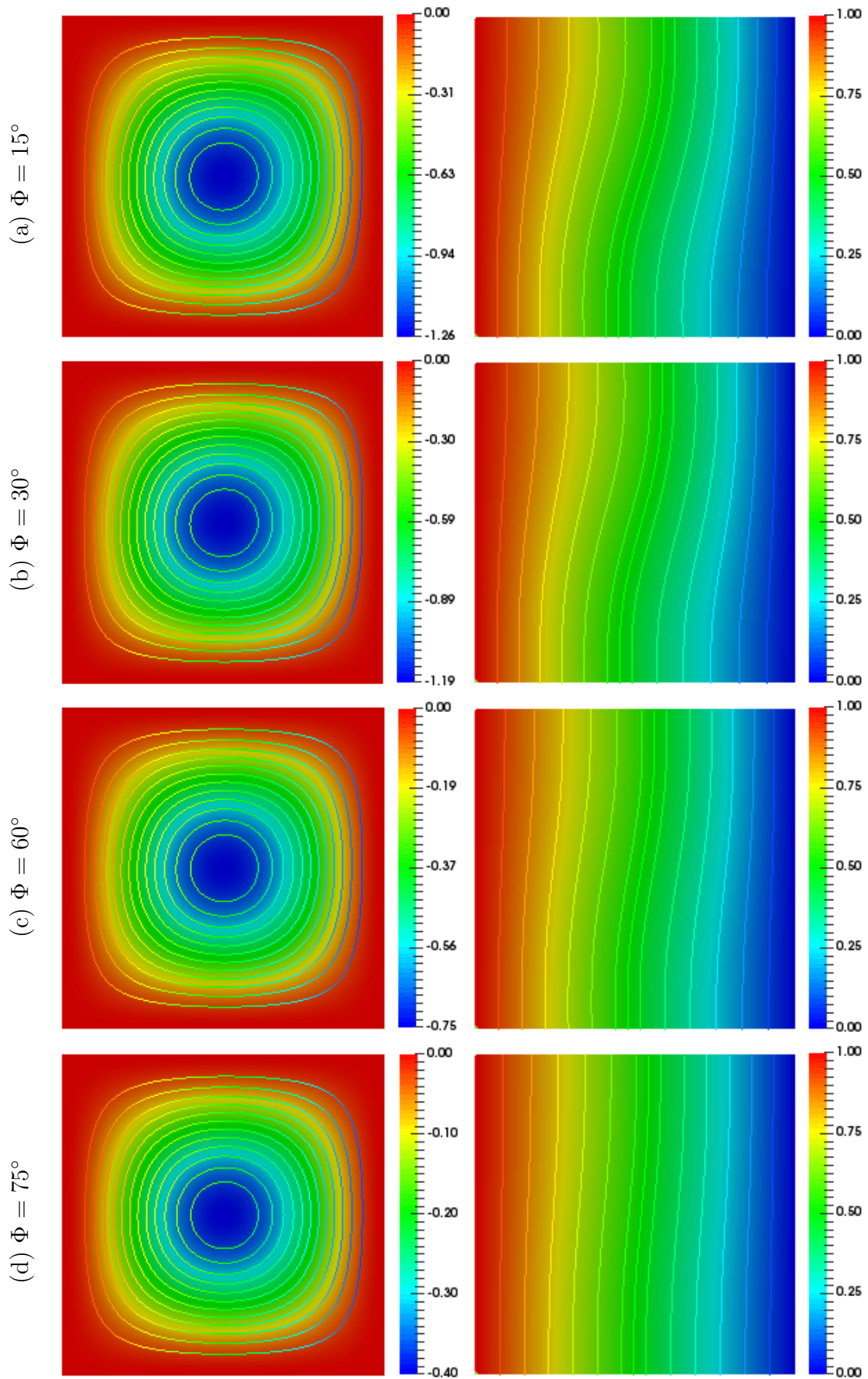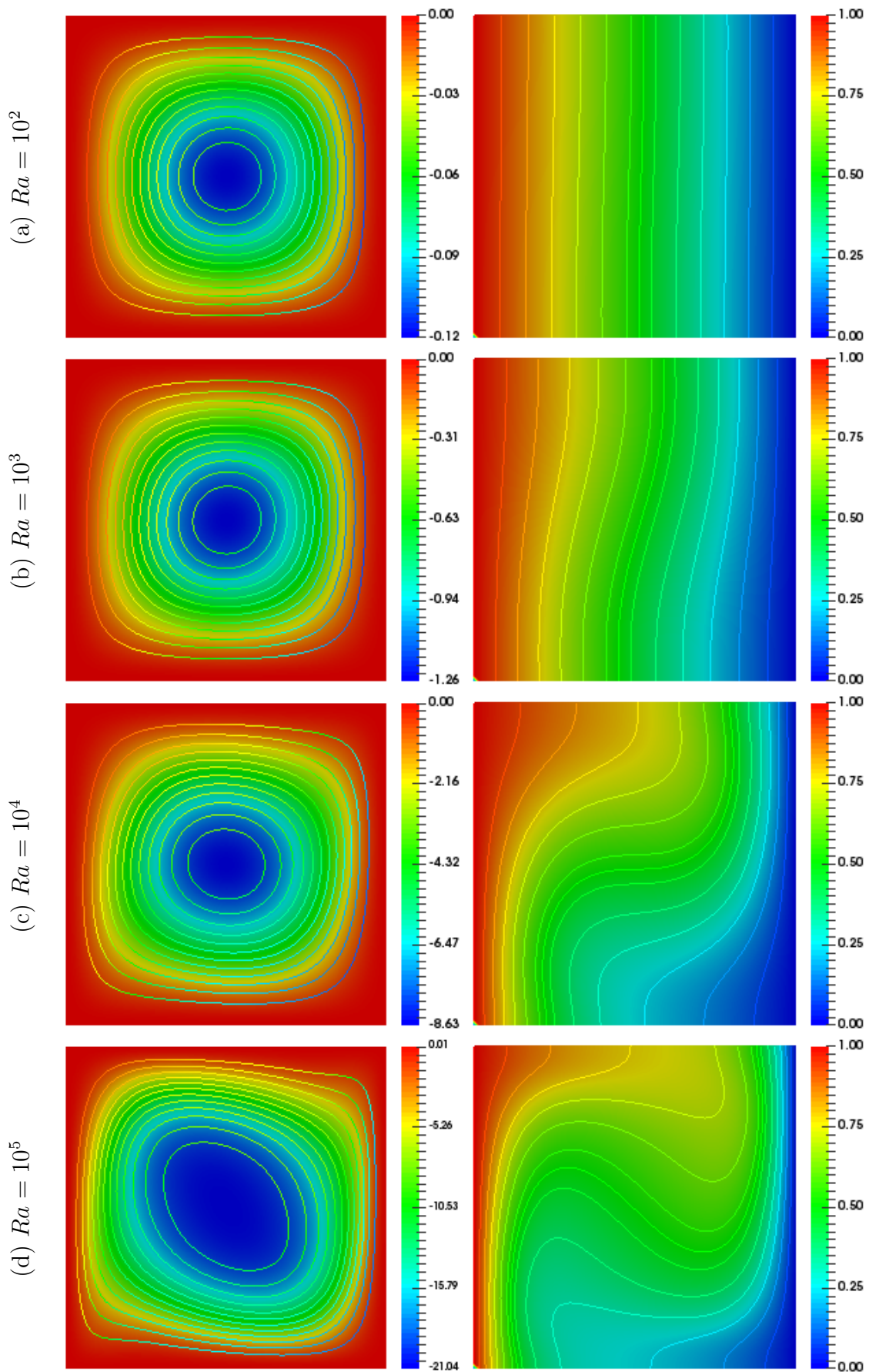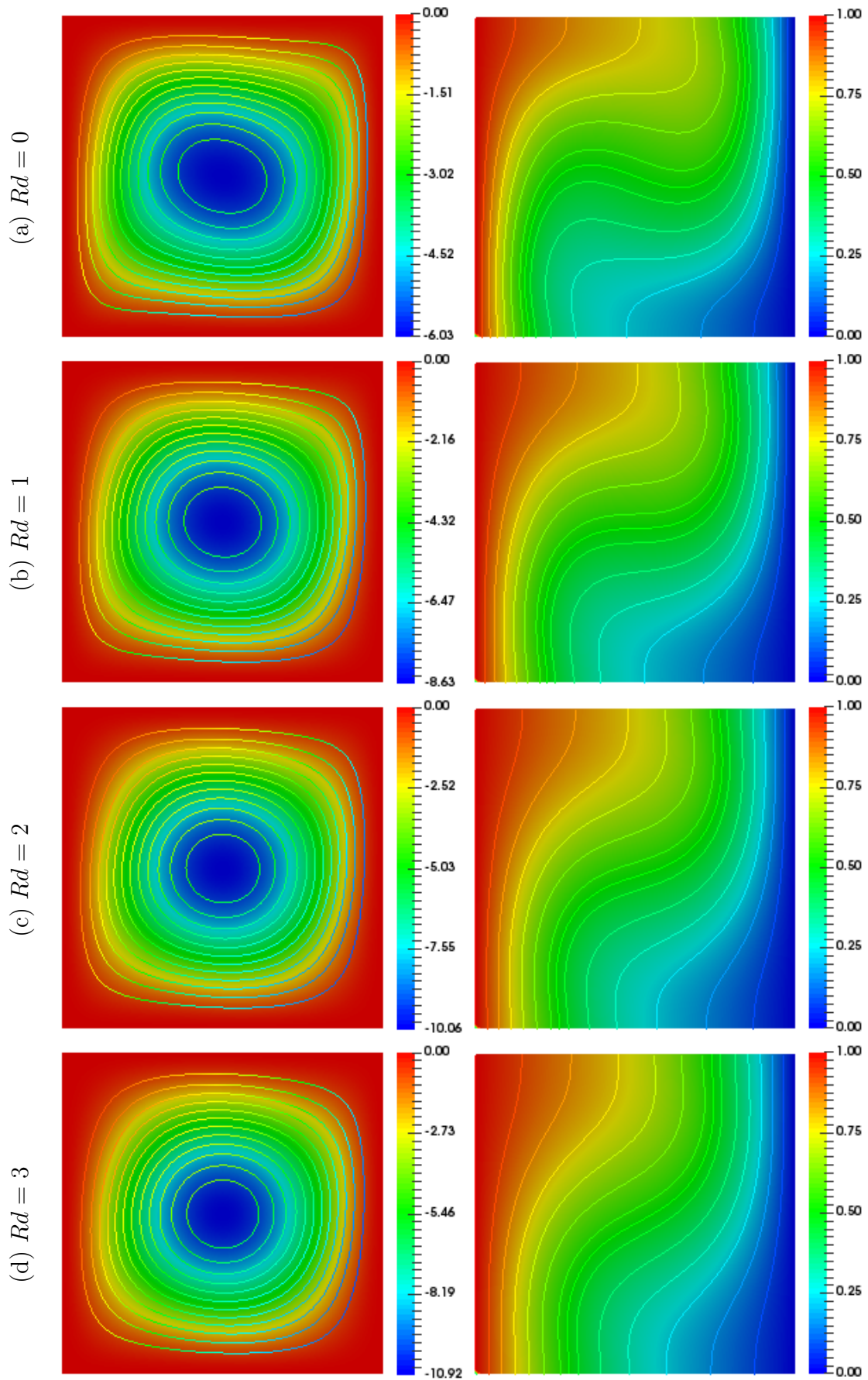
FIGURE 4.4: Impact of prandtl number (Pr) on streamlines (left) and isotherms (right) with parameters $\Phi = 15°$, $Nr = 1.1$, $Rd = 1$ and $Ra = 10^5$.
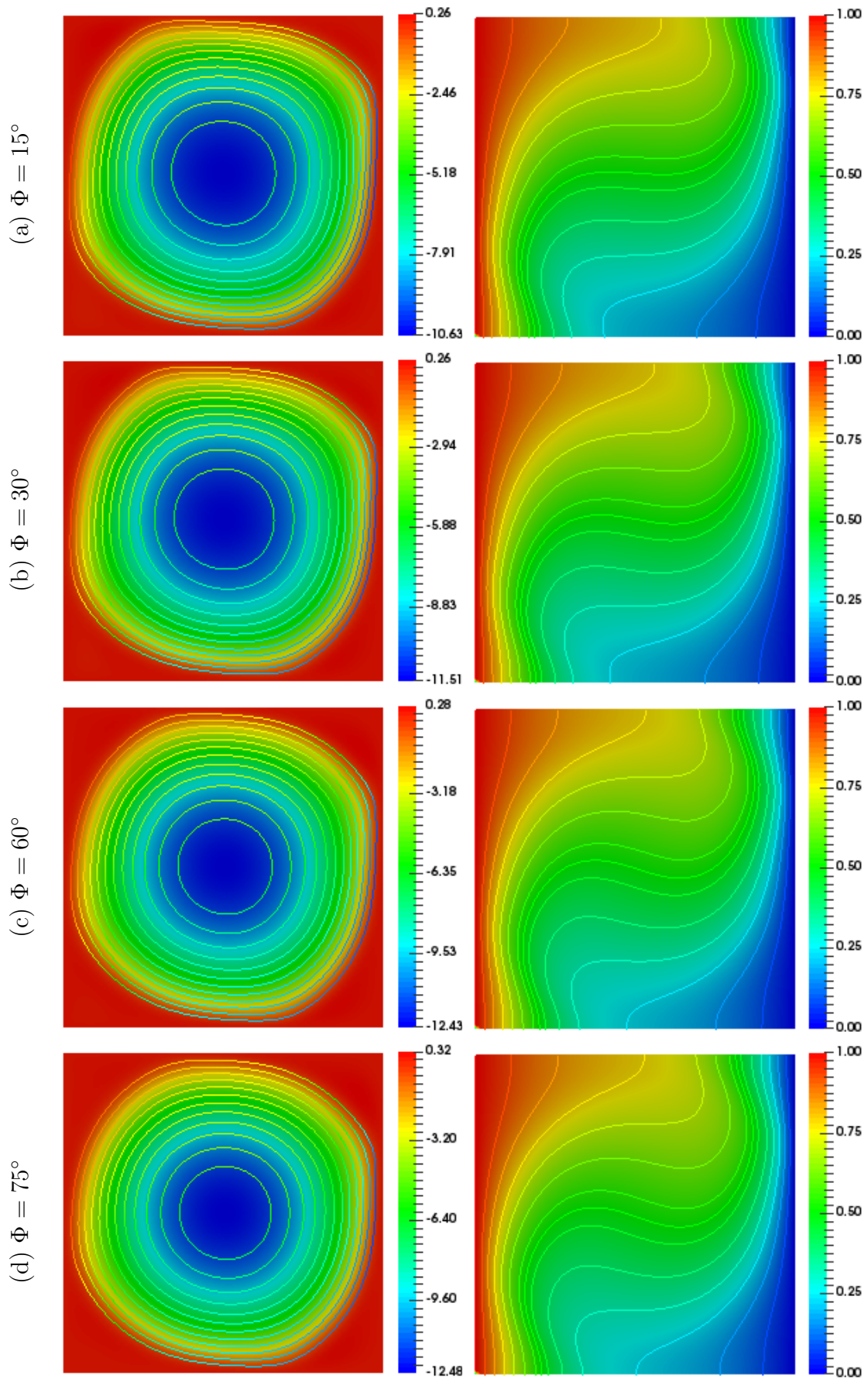
FIGURE 4.5: Impact of inclination angles (Φ) on streamlines (left) and isotherms (right) with parameters $Pr = 0.025$, $Nr = 1.1$, $Rd = 1$ and $Ra = 10^5$.
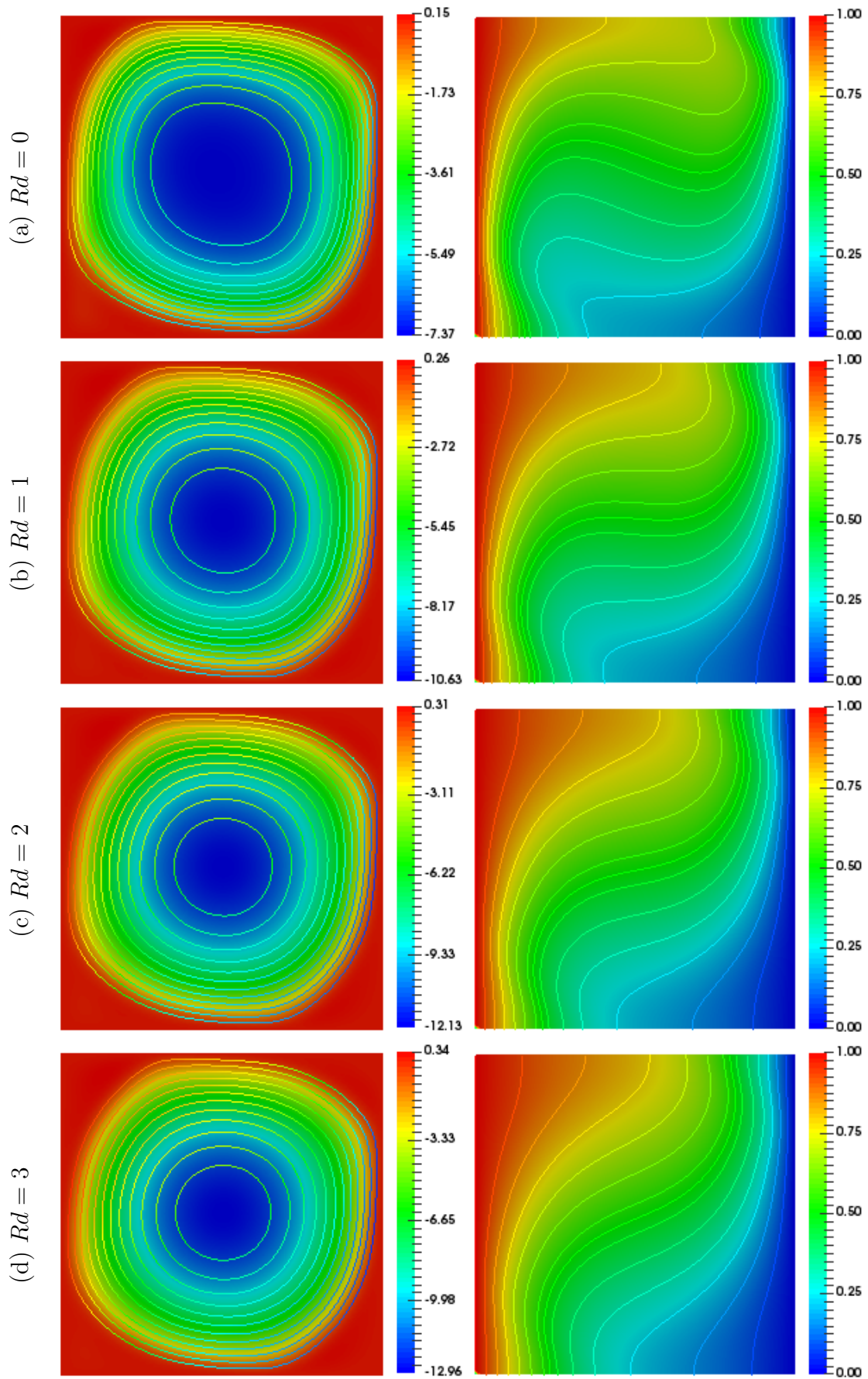
FIGURE 4.6: Impact of Radiation parameter (Rd) on streamlines (left) and isotherms (right) with $Pr = 0.025$, $\Phi = 15°$, $Nr = 1.1$ and $Ra = 10^5$.
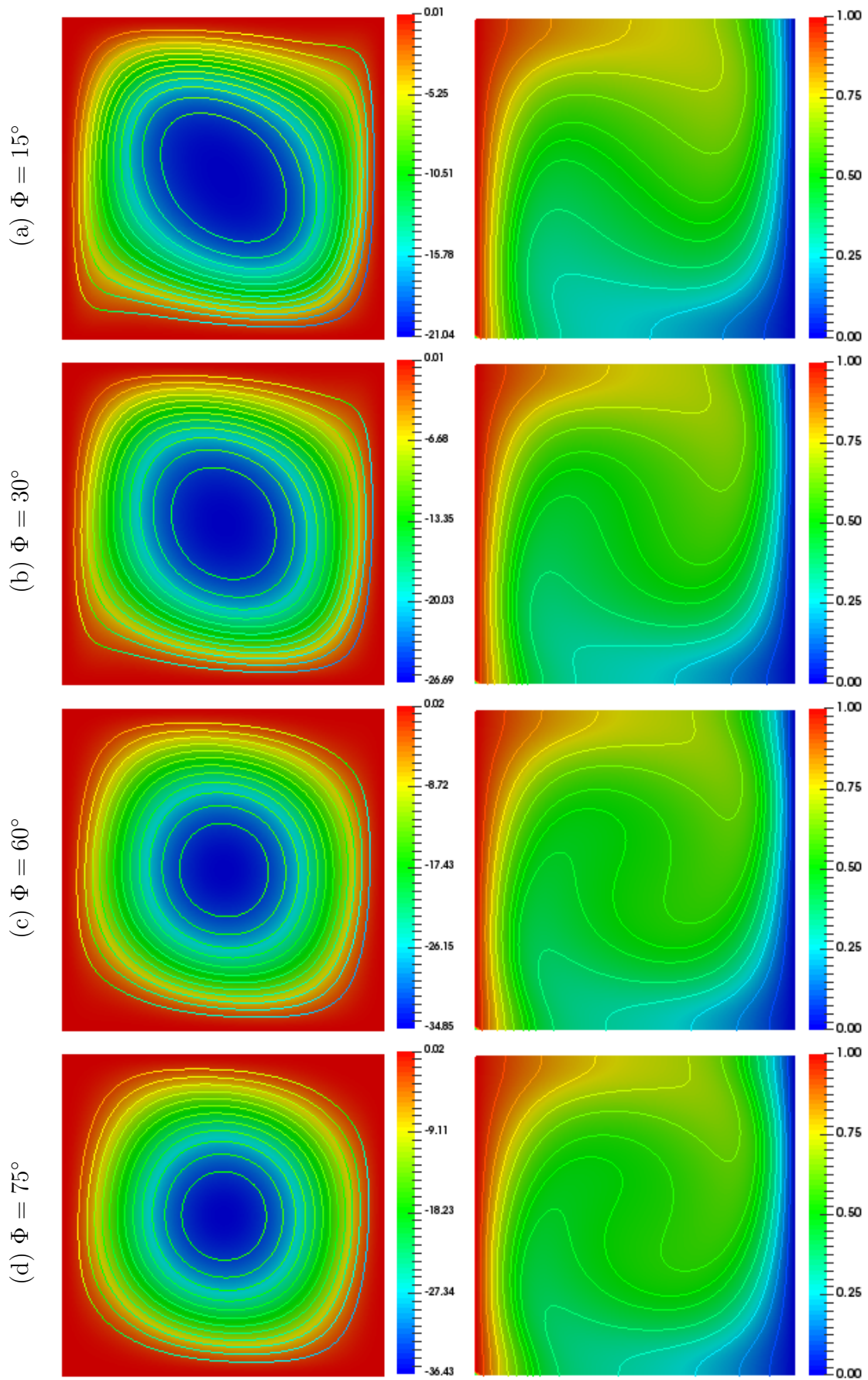
FIGURE 4.7: Impact of inclination angles (Φ) on streamlines (left) and isotherms (right) with parameters $Pr = 0.71$, $Nr = 1.1$, $Rd = 1$ and $Ra = 10^3$.

FIGURE 4.8: Influence of Rayleigh number ($Ra = 10^2 - 10^5$) on streamlines (left) and isotherms (right) with parameters $Pr = 0.71$, $\Phi = 15°$, $Nr = 1.1$ and $Rd = 1$.

FIGURE 4.9: Impact of Radiation parameter (Rd) on streamlines (left) and isotherms (right) with $Pr = 0.71$, $\Phi = 15°$, $Nr = 1.1$ and $Ra = 10^4$.

FIGURE 4.10: Impact of inclination angles (Φ) on streamlines (left) and isotherms (right) with parameters $Pr = 0.71$, $Nr = 1.1$, $Rd = 1$ and $Ra = 10^5$.
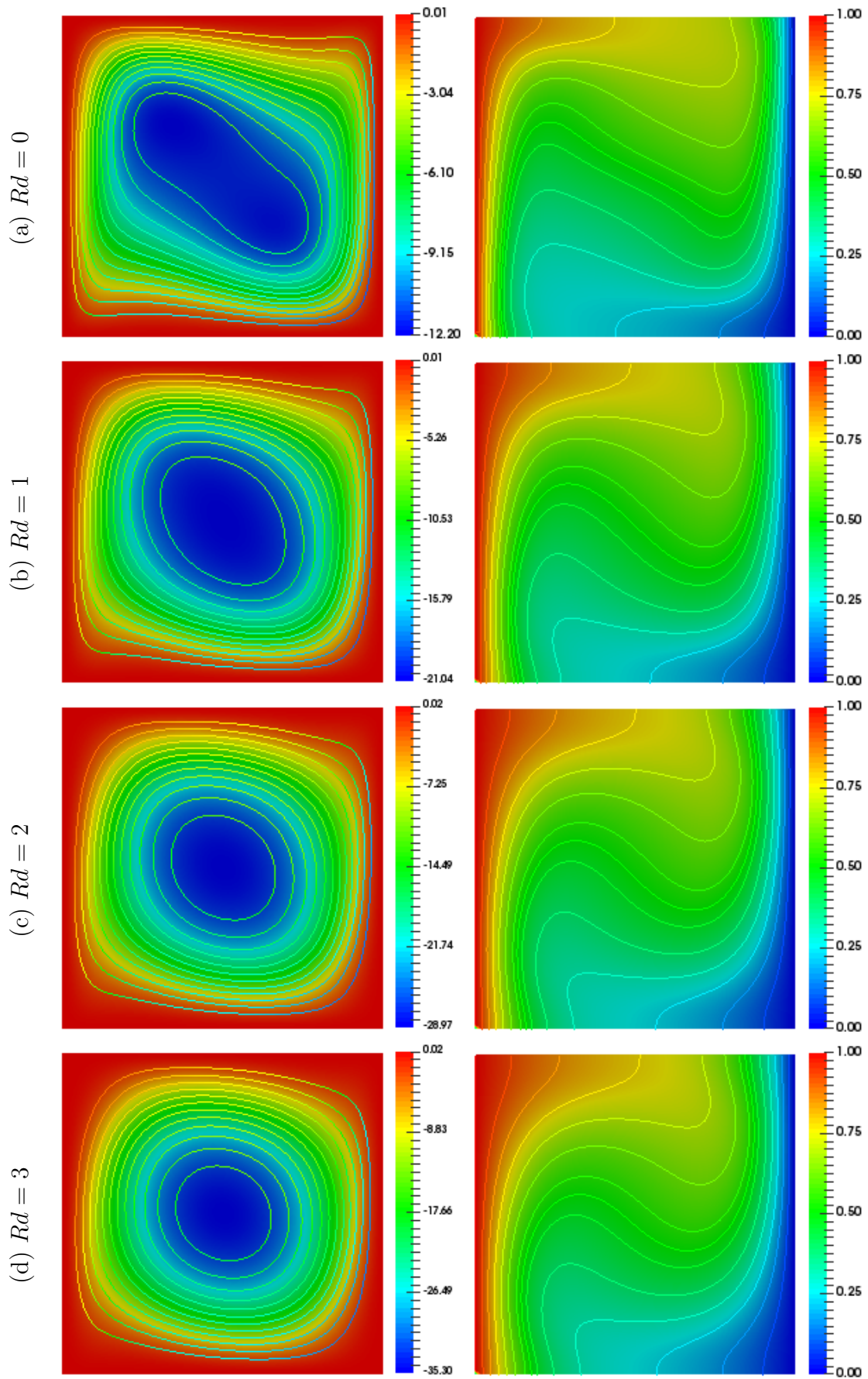
FIGURE 4.11: Impact of Rd on streamlines (left) and isotherms (right) with $Pr = 0.71$, $\Phi = 15°$, $Nr = 1.1$ and $Ra = 10^5$.
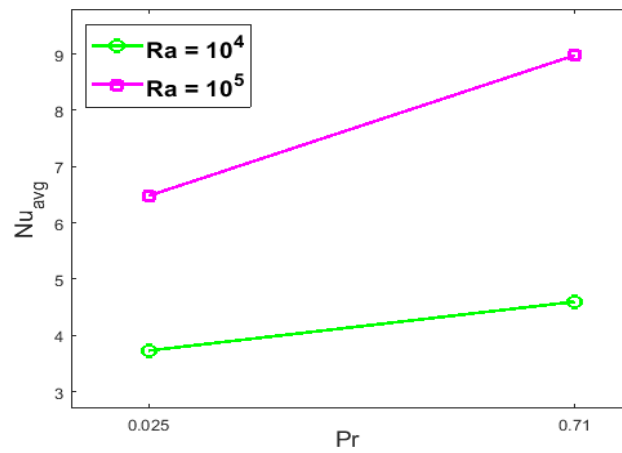
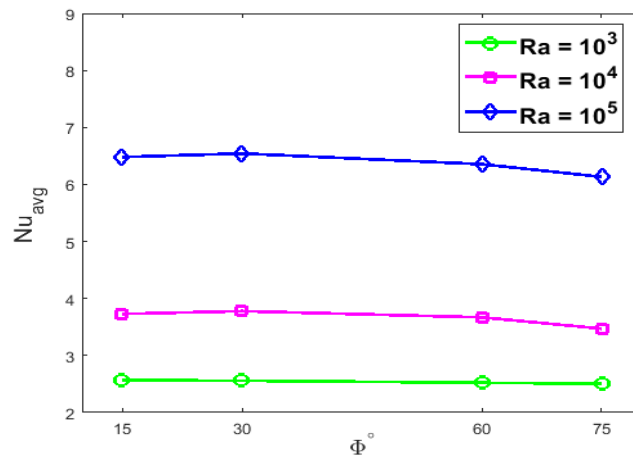FIGURE 4.12: Impact of Pr number on Nu_{avg} number w.r.t Ra with $Rd = 1$.

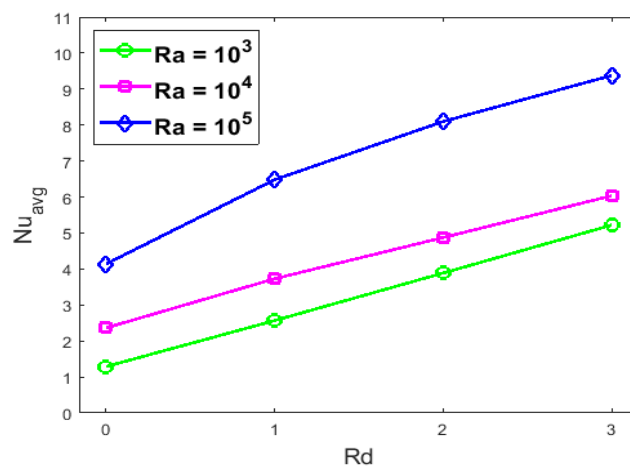FIGURE 4.13: Impact of Φ on Nu_{avg} number w.r.t Ra and $Pr = 0.025$.

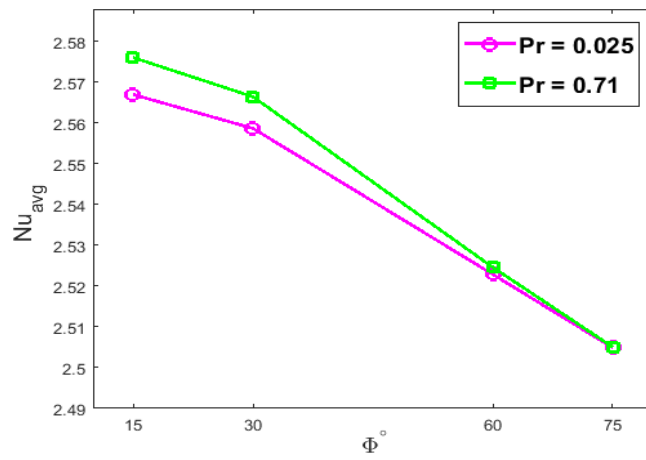FIGURE 4.14: Effect of Rd on Nu_{avg} number w.r.t Ra at fix $\Phi = 15°$.

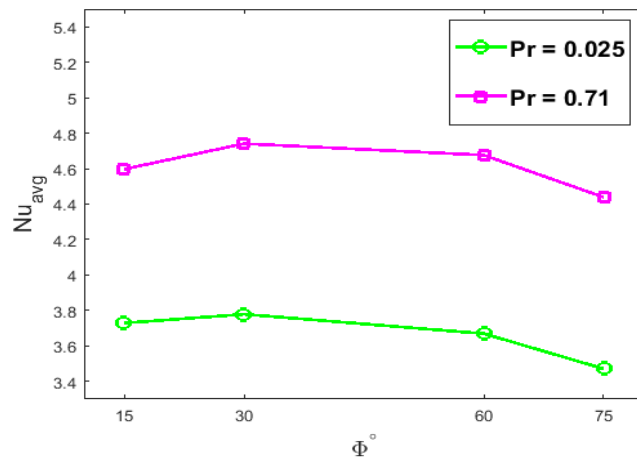FIGURE 4.15: Effect of Φ on Nu_{avg} number w.r.t Pr at fix $Ra = 10^3$.

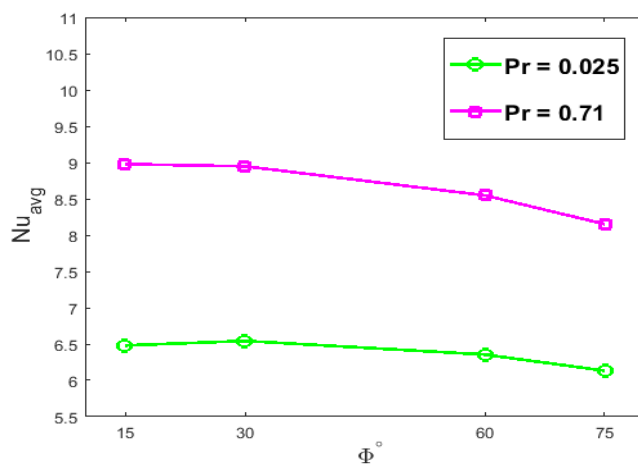FIGURE 4.16: Effect of Φ on Nu_{avg} number w.r.t Pr at fix $Ra = 10^4$.

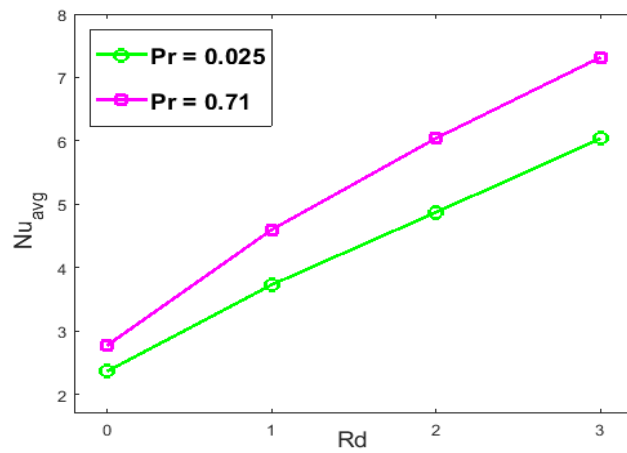FIGURE 4.17: Effect of Φ on Nu_{avg} number w.r.t Pr at fix $Ra = 10^5$.

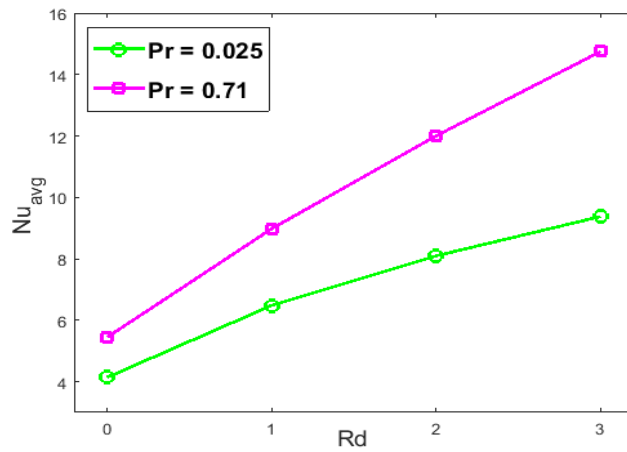FIGURE 4.18: Impact of Rd on Nu_{avg} number w.r.t Pr at fix $Ra = 10^4$.

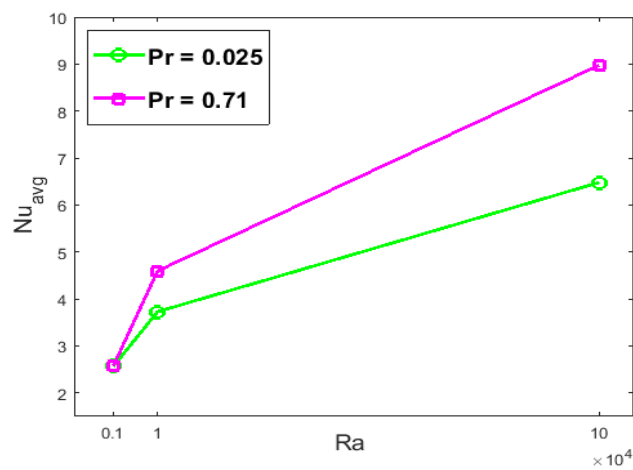FIGURE 4.19: Effect of Rd on Nu_{avg} number w.r.t Pr at fix $Ra = 10^5$.

FIGURE 4.20: Influence of Ra on Nu_{avg} number w.r.t Pr at fix $\Phi = 15°$.

Chapter 5

Conclusion

In this dissertation, the analysis of two dimensional steady and incompressible natural convection flow under the impact of non-linear thermal radiation is executed in a tilted square cavity. The cavity is considered with adiabatic walls at the top and bottom, hot wall on the left and cold wall on the right side. The governing dimensional PDEs developed for the heat exchange and fluid flow are first transformed into dimensionless PDEs by using an appropriate transformation. These equations are discretized and solved numerically by employing Galarkin finite elements technique. The finite element Q_2(biquadratic element) is used for velocity and temperature and P_1^{disc} is for pressure term. The impact of emerging parameters including Prandtl number, Rayleigh number and thermal radiation with inclination angles on the heat transfer and fluid flow has been thoroughly observed. Comparisons and results were found to be in good agreement discussed in literature. Graphical illustrations were presented to clarify the conclusions in clear way. Isotherms and streamlines were shown by the variation of inclination angle($\Phi = 15°, 30°, 60°, 75°$), Prandtle number ($Pr = 0.025, 6.2, 0.71$ and 998), radiational parameter ($Rd = 0$, 1, 2 and 3) and Rayleigh number ($Ra = 10^3, 10^4, 10^5$). The numerical simulations of the dimensionless velocity and temperature are analyzed by using the streamlines and isotherms, respectively, while the Nu_{avg} number is viewed by some useful plots against different physical parameters and inclination angle.

We extended the work of Basak *et al.* [14] with an idea of thermal radiatinal parameters to incorporate as shown in energy equation(4.4). The impact of radiation parameter on the flow by means of streamlines and isotherms has been observed. The average Nusselt number against the heat radiation parameter is also analyzed by Matlab plots. Concluding all valuable results obtained through numerical simulations leads to the following points.

- The convective forces for high Rayleigh number ($Ra \geq 10^4$) enhanced inside the cavity. At high Rayleigh number, an increment in the flow of fluid and heat is observed due to the strong convection for all considered cases of Rd. Large values are noticed for the magnitude of streamfunction at the center of the cavity irrespective of the prandtl number (Pr) and inclination angle (Φ).

- With enhancement in Rd yields augmentation in rate of convective flow, attenuation in the size of thermal boundary layer as well as convective cores. For excessive values of Rd, the conduction of heat dominating the mechanism of heat transfer and on the otherhand reduces in the inclination of isotherms.

- The intensity of flow and rate of heat transfer are greater in magnitude for air but lower for mercury.

- Nu_{avg} increases with enhancement in Pr, Rd and Ra, but decreases for increasing values of inclination angle (Φ).

5.1　Future Recommendations

The analysis performed in this thesis can be further extended in the following directions:

1. Analyzing the impact of porous media.

2. To perform the non-stationary simulation.

3. Apply the higher order finite elements in space.

4. Apply the Galerkin discretization scheme for temporal discretization.

Bibliography

[1] G. D. V. Davis., "Natural convection in a square cavity: A benchmark numerical solutions," *International Journal for Numerical Method in Fluids*, vol. 3, pp. 261–282, 2009.

[2] F. Kuznik, J. Vareilles, G. Rusaouen, and G. Krauss., "A double-population Lattice Boltzmann method with non-uniform mesh for the simulation of natural convection in a square cavity," *International Journal of Heat and Fluid Flow*, vol. 28, pp. 862–870, 2007.

[3] R. Djebali, M. E. Ganoui, H. Sammouda, and R. Bennacer., "Some benchmarks of a side wall heated cavity using Lattice Boltzmann approach," *Fluid Dynamics and Material Processing*, vol. 83, pp. 51–71, 2014.

[4] H. N. Dixit and V. Babu., "Simulations of high Raleigh number natural convection in a square cavity using the Lattice Boltzmann method," *International Journal of Heat and Mass Transfer*, vol. 49, pp. 727–739, 2006.

[5] H. F. Öztop, Y. Varol, and A. Koca., "Experimental investigation of cooling of heated circular disc using inclined circular jet," *International Communications in Heat and Mass Transfer*, vol. 38, pp. 990–1001, 2010.

[6] Y. C. Pei., "Thermoelastic damping inrotating flexible micro-disk," *International Journal of Mechanical Sciences*, vol. 61, pp. 52–64, 2012.

[7] M. Rahimi, I. Owen, and J. Mistry., "Thermal stresses in boiler tubes arises from high-speed jets," *International Journal of Mechanical Sciences*, vol. 45, pp. 995–1009, 2003.

[8] M. Turkyilmazoglu., "Exact solution for the incompressible viscous magneto-hydrodynamics of a porous rotating disk flow with hall current," *International Journal of Mechanical Sciences*, vol. 56, pp. 86–95, 2012.

[9] H. Aminfar, M. Mohammadpourfard, and F. Moseni., "Numerical investigation of thermocapillary and buoyancy driven convection of nanofluids in a floating zone," *International Journal of Mechanical Sciences*, vol. 65, pp. 147–156, 2012.

[10] S. S. Azimi and M. Kalbasi., "Numerical study of dynamic thermal conductivity of nanofluid in the forced convective heat transfer," *Applied Mathematical Modelling*, vol. 38(4), pp. 1373–1384, 2014.

[11] M. Kalteh., "Investigating the effect of various nanoparticle and base liquid types on the nanofluids heat and fluid flow in a microchannel," *Applied Mathematical Modelling*, vol. 37, pp. 18–19, 2013.

[12] M. M. Ganzoralli and L. F. Milanez., "The effects of MHD and temperature dependent viscosity on the flow of non-Newtonian nanofluid in a pipe: Analytical solutions," *Appl. Math*, vol. 37(3), pp. 1451–1467, 2013.

[13] R. K. Tiwari and M. K. Das., "Heat transfer augmentation in a two-sided lid-driven differentially heated square cavity utilizing nanofluids," *International Journal of Heat and Mass Transfer*, vol. 50, pp. 2002–2018, 2007.

[14] T. Basak, A. Kumar, and S. Roy., "Finite element simulations on heat flow visualization and entropy generation during natural convection in inclined square cavities," *International Communication in Heat and Mass Transfer*, vol. 51, pp. 1–8, 2014.

[15] H. Ozoe, H. Sayama, and S. W. Churchill., "Natural convection in an inclined square channel," *International Journal of Heat and Mass Transfer*, vol. 17, pp. 401–406, 1974.

[16] J. Rasoul and P. Prinos., "Natural convection in an inclined enclosure," *International Journal of Numerical Methods for Heat and Fluid Flow*, vol. 7, pp. 438–478, 1997.

[17] I. Catton, P. S. Ayyaswamy, and R. M. Clever., "Natural convection flow in a finite rectangular slot arbitrarilu oriented with respect to the gravity vector," *International Journal of Heat and Mass Transfer*, vol. 32, pp. 173–184, 1974.

[18] K. A. Farhny and A. Kuran., "Numerical study of double diffusive natural convective heat and mass transfer in an inclined rectangular cavity filled with porous medium," *International Communications in Heat and Mass Transfer*, vol. 39, pp. 174–181, 2012.

[19] F. J. Hamady, J. R. Lloyd, H. Q. Yang, and K. T. Yang., "Study of local natural convection heat transfer in an inclined enclosure," *International Journal of Heat and Mass Transfer*, vol. 32, pp. 1697–1708, 1989.

[20] G. S. Shiralker and C. L. Tien., "A numerical study of the effect of a vertical temperature difference imposed on a horizontal enclosure," *International Journal of Heat and Fluid Flow*, vol. 28, pp. 1492–1506, 2007.

[21] M. M. Ganzoralli and L. F. Milanez., "Natural convection in rectangular enclosure heated from below and symmetrically cooled from the sides," *Communications inNonlinear Science and Numerical Simulation*, vol. 15, pp. 1501–1510, 2010.

[22] K. Khanafer, A. Azmi, and I. Pop., "Non-Darcian effects on natural convection heat transfer in a wavy porous enclosure," *International Journal of Heat and Mass Transfer*, vol. 52, pp. 1887–1896, 2009.

[23] F. Selimefendigil and H. F. Öztop., "Numerical study of MHD mixed convection in a nanofluid filled lid driven square enclosure with a rotating cylinder," *International Journal of Heat and Mass Transfer*, vol. 78, pp. 741–754, 2014.

[24] E. A. Nada., "Applications of nanofluids for heat transfer enhancement of separated flows," *Heat and Fluid Flow*, vol. 29, pp. 242–249, 2008.

[25] C. Cianfrini, P. P. Corcione, and M. Dell'Omo., "Natural convection in tilted square cavities with differentially heated opposed walls," *International Journal of Mechanical Sciences*, vol. 44(5), pp. 441–451, 2005.

[26] K. Mehmood, S. Hussain, and M. Sagheer, "Numerical simulation of MHD mixed convection in aluminawater nanofluid filled square porous cavity using KKL model: Effects of non-linear thermal radiation and inclined magnetic field," *Journal of Molecular Liquids*, vol. 238, pp. 485–498, 2017.

[27] B. C. Shekar and N. Kishan, "Finite element analysis of natural convective heat transfer in a porous square cavity filled with nanofluids in the presence of thermal radiation." *Journal of Physics*, vol. 662, pp. 1097–1103, 2015.

[28] T. R. Mahapatra, D. Pal, and S. Mondal., "Natural convection in a lid-driven square cavity filled with Darcy-Forchheimer porous medium in the presence of thermal radiation," *International Journal of Nonlinear Science*, vol. 11, pp. 366–379, 2011.

[29] M. Ghalambaz, M. Sabour, and I. Pop., "Free convection in a square cavity filled by a porous medium saturated by a nanofluid: Viscous dissipation and radiation effects," *Engineering Science and Technology, an International Journal*, vol. 19, pp. 1244–1253, 2016.

[30] M. Sheikholeslami, T. Hayat, and A. Alsaedi., "MHD free convection of alumina-water nanofluid considering thermal radiation: A numerical study," *International Journal of Heat and Mass Transfer*, vol. 96, pp. 513–524, 2016.

[31] S. Hussain, F. Schieweck, and S. Turek, "Efficient newton multigrid solution techniques for higher order space time Galerkin discretizations of incompressible flow," *Applied Numerical Mathematics*, vol. 83, pp. 51–71, 2014.

[32] J. H. Ferziger and M. Peric, "Computational methods for fluid dynamics," *Springer*, vol. 3, 2002.

[33] D. Misra and A. Sarkar, "Finite element analysis of conjugate natural convection in a square enclosure with a conducting vertical wall," *Computer Methods in Applied Mechanics and Engineering*, vol. 141, pp. 205–219, 1997.

[34] R. Lohner, "Applied computational fluid dynamics techniques," *Wiley*, vol. 2, 2008.

[35] A. Bejan, "Convection heat transfer," *Wiley*, vol. 4, 2013.